

Boosting Adversarial Transferability with Low-Cost Optimization via Maximin Expected Flatness

Chunlin Qiu, Ang Li, Yiheng Duan, Shenyi Zhang, Yuanjie Zhang,
Lingchen Zhao, Qian Wang, *Fellow, IEEE*

Abstract—Transfer-based attacks craft adversarial examples on white-box surrogate models and directly deploy them against black-box target models, offering model-agnostic and query-free threat scenarios. While flatness-enhanced methods have recently emerged to improve transferability by enhancing the loss surface flatness of adversarial examples, their divergent flatness definitions and heuristic attack designs suffer from unexamined optimization limitations and missing theoretical foundation, thus constraining their effectiveness and efficiency. This work exposes the severely imbalanced exploitation-exploration dynamics in flatness optimization, establishing the first theoretical foundation for flatness-based transferability and proposing a principled framework to overcome these optimization pitfalls. Specifically, we systematically unify fragmented flatness definitions across existing methods, revealing their imbalanced optimization limitations in over-exploration of sensitivity peaks or over-exploitation of local plateaus. To resolve these issues, we rigorously formalize average-case flatness and transferability gaps, proving that enhancing zeroth-order average-case flatness minimizes cross-model discrepancies. Building on this theory, we design a Maximin Expected Flatness (MEF) attack that enhances zeroth-order average-case flatness while balancing flatness exploration and exploitation. Extensive evaluations across 22 models and 24 current transfer-based attacks demonstrate MEF's superiority: it surpasses the state-of-the-art PGN attack by 4% in attack success rate at half the computational cost and achieves 8% higher success rate under the same budget. When combined with input augmentation, MEF attains 15% additional gains against defense-equipped models, establishing new robustness benchmarks. Our code is available at <https://github.com/SigneQiu/MEFAttack>.

Index Terms—Adversarial attack, Black-box attack, Adversarial transferability, Loss surface flatness, Loss landscape

I. INTRODUCTION

ADVERSARIAL examples [10]–[13] pose a significant security threat to deep neural networks (DNNs). By introducing imperceptible perturbations to benign inputs, attackers can craft adversarial examples that mislead DNNs into producing erroneous predictions. Early adversarial attacks primarily operated under two paradigms: white-box attacks that require full access to the target model's architecture and parameters, such as FGSM [14], PGD [15], and C&W [13], and query-based grey-box attacks that rely on iterative adversarial direction estimation through repeated model queries, as seen in Boundary Attack [16], SimBA [17], and HSJA [18]. While effective, these methods face critical deployment barriers: white-box attacks assume unrealistic access to victim

Chunlin Qiu, Ang Li, Yiheng Duan, Shenyi Zhang, Yuanjie Zhang, Lingchen Zhao, Qian Wang are with Key Laboratory of Aerospace Information Security and Trusted Computing, Ministry of Education, School of Cyber Science and Engineering, Wuhan University, Wuhan 430072, China (e-mail: {chunlinqiu, anglil, yihengduan, shenyizhang, yuanjiezhang, lc Zhao, qianwang}@whu.edu.cn).

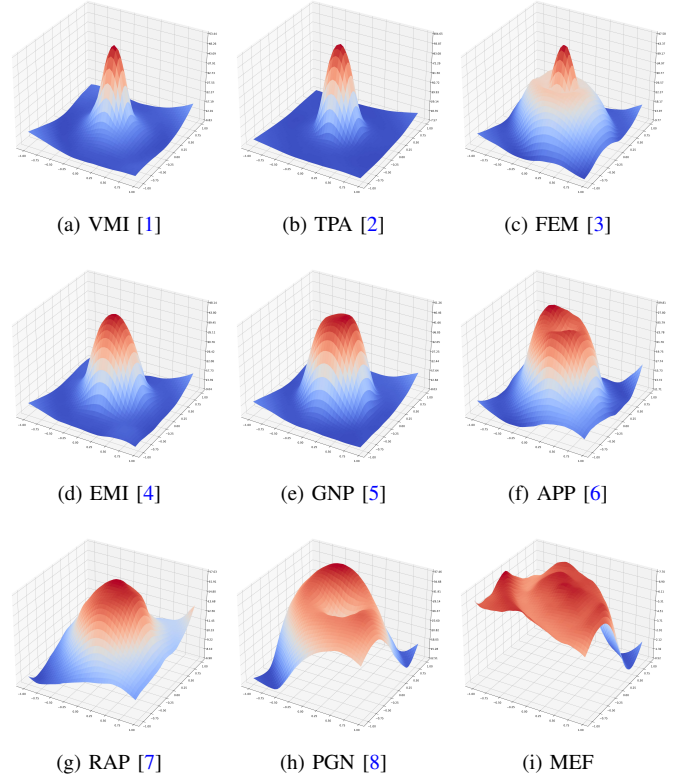


Fig. 1. Visualization of adversarial loss landscapes for nine attacks on Res-50 [9]. The loss surfaces is constructed by perturbing adversarial examples along two random directions. Our MEF attack achieves the flattest loss landscape, indicating superior flatness-based transferability.

models, while query-based methods incur prohibitive query overhead, making them impractical in real-world scenarios.

Transfer-based attacks [1], [2], [19]–[24] overcome these limitations by crafting adversarial examples on surrogate models and directly transferring them to black-box targets. This paradigm eliminates both dependency on target model's internals and query interactions, making it a practical threat to real-world systems. Among these attacks, a recent class of flatness-enhanced methods [2], [3], [7], [8] has emerged as a promising direction by linking the geometric flatness of the adversarial loss landscape to adversarial transferability. Flatness-enhanced methods craft adversarial examples with flatter neighborhood loss landscapes, enhancing cross-model robustness and achieving state-of-the-art transferability [8].

Despite their empirical success, flatness-enhanced methods face two fundamental limitations. Firstly, they adopt fragmented flatness definitions without systematic comparison, failing to discern their inherent advantages and critical flaws. Secondly, they rely on the empirically assumed but unproven

connection between flatness and transferability [3], [5], [7], [8], leading to non-rigorous and suboptimal optimization.

To address these limitations, we first unify fragmented flatness definitions within a multi-order framework that differentiates between worst-case and average-case flatness. Through experiments, we demonstrate that worst-case flatness optimization over-explores high-curvature regions and average-case methods over-exploit suboptimal plateaus, two critical flaws responsible for the performance bottleneck in existing attacks. We further establish the first theoretical proof linking flatness to transferability, formalizing that enhancing multi-order average-case flatness reduces cross-model discrepancies. Our theoretical analysis certifies zeroth-order flatness as the dominant transferability source, paving the way for high-transferability attacks with reduced computational costs.

Based on the empirical and theoretical analysis, we propose the Maximin Expected Flatness (MEF) attack to enhance adversarial transferability while reducing computational cost. Our key insight is to leverage the complementary strengths of average-case and worst-case flatness optimization, where average-case methods stabilize local exploitation while worst-case strategies preserve global exploration capability. MEF attack explicitly optimizes *zeroth-order worst-neighborhood average flatness*, a unified metric that internally computes neighborhood-level average-case flatness to stabilize local exploitation and externally identifies worst-case regions to guide global exploration. MEF implements this via gradient-guided neighborhood conditional sampling (NCS) for efficient worst-region identification and gradient balancing optimization (GBO) that reuses gradients across stages, reducing computation by 50% while enhancing transferability. By coupling these mechanisms, MEF achieves flattest loss landscape (as shown in Fig. 1) and enhanced adversarial transferability. Third-party evaluation on the widely-adopted [TransferAttack](#) benchmark shows MEF dominates 22 gradient-based methods as the new leader. Our main contributions are summarized as follows:

- We unify fragmented flatness definitions across existing methods and establish the first theoretical foundation of flatness-based transferability, connecting multi-order average-case flatness with adversarial transferability.
- We propose Maximin Expected Flatness (MEF) attack, together with Neighborhood Conditional Sampling (NCS) and Gradient Balancing Optimization (GBO) to boost adversarial transferability with efficient computation.
- Extensive experiments and third-party evaluation¹ validate the superior effectiveness of MEF attack, surpassing the SOTA PGN [8] attack by 4% in attack success rate on average at half the computational cost and achieves 8% higher success rate under the same budget.

The paper is organized as follows. Sec. II reviews transfer-based attacks and defenses. Sec. III unifies fragmented flatness definitions and reveals the limitations in current flatness optimization. Sec. IV establishes the theoretical foundation for flatness-based transferability. Sec. V introduces Maximin Expected Flatness (MEF) attack. Sec. VI conducts extensive evaluation experiments and Sec. VII concludes the paper.

II. RELATED WORK

This section systematically reviews adversarial machine learning literature through two lenses: (1) we survey adversarial attacks with emphasis on transfer-based attacks, and (2) analyze various adversarial defense mechanisms, including both reactive and proactive defenses.

A. Adversarial Attacks

We first give the formal definition of adversarial attacks and then introduce various transfer-based attacks. Adversarial attacks craft perturbed examples $\mathbf{x}^{adv} \in B_\epsilon(\mathbf{x}) = \{\mathbf{x}' : \|\mathbf{x}' - \mathbf{x}\|_p \leq \epsilon\}$ to fool a neural network $\mathcal{F} : \mathcal{X} \rightarrow \mathcal{Y}$, where $\mathbf{x} \in \mathcal{X}$ is the clean input with label $y \in \mathcal{Y}$. The attack objective:

$$\max_{\mathbf{x}^{adv} \in B_\epsilon(\mathbf{x})} J(\mathbf{x}^{adv}, y; \mathcal{F}),$$

where $J : \mathcal{X} \times \mathcal{Y} \rightarrow \mathbb{R}$ denotes the adversarial loss function. Following standard practice, we adopt the ℓ_∞ -norm ($p = \infty$) for perturbation constraints. For notation simplicity, we may write $J(\mathbf{x}) \triangleq J(\mathbf{x}, y; \mathcal{F})$. An intriguing property of adversarial examples is transferability, where adversarial examples crafted on surrogate model \mathcal{F} also deceive the unknown target model \mathcal{F}' , enabling black-box attacks. Transfer-based attacks can be roughly divided into *data-driven methods*, *model-driven methods* and *optimization-driven methods*, as follows.

Data-driven Methods. Data-driven methods [19], [20], [22], [25] boost adversarial transferability by aggregating gradients over multiple augmented variants through data transformation strategies. The key distinction between these methods centers on the specific transformation operators. DI [19] optimizes over resized images, TI [20] applies spatial shifting, and SI [22] manipulates pixel scaling. Beyond these single-input spatial transformations, Admix [25] enhances diversity by blending cross-category images, while SSA [26] perturbs frequency domains to break spatial locality. To further amplify input variety, composite strategies integrate multiple transformations [27], [28]. However, such strategies incur significant computational overheads and induce semantic distortions [29], ultimately compromising their effectiveness.

Model-driven Methods. Model-driven methods [23], [30]–[33] exploit geometric priors [33] in surrogate models' feature spaces to enhance adversarial transferability, primarily through two strategies: model ensemble aligns heterogeneous architectures via joint perturbation optimization to amplify spectral commonality with victims [31], [32], while surrogate refinement adversarially tunes surrogates or aligns gradients to reshape decision boundaries [23], [30]. However, model ensemble scales linearly with surrogates' computational costs, and refinement struggles on large datasets due to complex regularization, limiting both to small-scale applications [34].

Optimization-driven Methods. Optimization-driven methods [7], [21], [24], [35], enhance transferability by redesigning optimization objectives [24], [35] or algorithms [21], [36]. Advanced Objective strategies replace cross-entropy loss with feature discrepancy losses that align surrogate-victim model features [24], [35]. Generative Modeling strategies leverage generative networks to synthesize perturbations without iterative updates [36]. Gradient Stabilization strategies retain

¹Available in: <https://github.com/Trustworthy-AI-Group/TransferAttack>

simple losses but refines gradient dynamics via momentum [4], [21], [22] or variance reduction [1]. Compared to the former two paradigms requiring complex losses or architectures, gradient stabilization strategies achieve transferability with minimal complexity, avoiding auxiliary data and models.

Recent advances in gradient stabilization attacks have seen the emergence of flatness-enhanced methods, which propose that adversarial examples within flatter loss regions exhibit stronger transferability. These methods diverge into two strategies: those optimizing *average-case flatness* by aggregating gradients over local neighborhoods (e.g., FEM [3], APP [6]), and those pursuing *worst-case flatness* by minimizing gradient peaks (PGN [8]) or maximizing minimal loss (RAP [7]). However, existing works adopt fragmented flatness definitions while relying on empirically assumed correlations between flatness and transferability, obscuring theoretical understanding of their inherent limitations. Our work bridges this gap by establishing unified flatness-transferability guarantees and adaptive optimization that harmonizes both flatness criteria.

B. Adversarial Defenses

Adversarial defenses can be categorized into two paradigms: *proactive defenses* that strengthen model robustness through architectural or parametric adjustments, and *reactive defenses* that deploy external mechanisms to sanitize or detect adversarial inputs without modifying model parameters.

Proactive Defenses. Proactive defenses aim to intrinsically harden model parameters against adversarial perturbations. The dominant approach, adversarial training (AT) [15], [37], reformulates robust model optimization as a min-max optimization problem, where the inner maximization generates perturbations to craft challenging adversarial examples, while the outer minimization enforces the model to correctly classify these perturbed samples. Variants like ensemble adversarial training (EAT) [38] augment robustness through multi-model perturbations during training, strengthening defense against cross-architecture transfer attacks. In contrast to AT's empirical robustness, randomized smoothing [39] provides certifiable robustness by injecting Gaussian noise into inputs and certifying predictions over perturbed samples. While this method theoretically guarantees robustness within a certified radius, such radii are often smaller than adversarial perturbations defended by AT, rendering it ineffective against practical adversarial threats despite its theoretical appeal [40].

Reactive Defenses. Reactive defenses mitigate adversarial attacks without modifying model parameters. Adversarial purification [41]–[43] projects inputs onto clean data manifolds using generative models [41], [43] or denoisers [42], while adversarial detection identifies adversarial examples via activation anomalies or confidence thresholds [44]. These strategies offer plug-and-play deployment but suffer from two limitations: purification efficacy depends on generative model capacity [45], and detectors can be bypassed by adaptive attacks that mimic clean data statistics [46].

Our attack demonstrates strong transferability against both proactive defenses [38], [39] and reactive defenses [41]–[43], effectively bypassing their protection mechanisms through flatness-enhanced perturbation crafting.

III. LIMITATIONS IN FLATNESS ENHANCEMENT

The heuristic adoption of flatness concepts in flatness-enhanced methods lacks rigorous theoretical grounding while suffering from absence of systematic comparisons between flatness metrics, which constrains their effectiveness and efficiency. In this section, we first formalizes flatness as a measurable geometric property, resolving definitional ambiguities across existing methods. Then we identify two inherent limitations in current flatness-enhanced methods. Finally, we distill the critical yet understudied challenges in balancing local exploitation and global exploration for real-world deployment.

A. K -th Order Flatness

In this section, we introduce the formal definitions of k -order worst- and average-case flatness metrics, establishing a unified taxonomy for flatness enhancement and enabling systematic classification of six flatness-enhanced methods.

The study of loss landscape flatness originated in model generalization theory, where flatter minima were shown to correlate with improved generalization performance [49]–[51]. In model generalization, the most popular mathematical definition of flatness, proposed by SAM [49], considers the maximal loss value within a radius, termed the *zeroth-order worst-case flatness*. Building upon this foundation, Gradient norm Aware Minimization (GAM) [51] extends this framework to *first-order worst-case flatness*, a stricter geometric criterion that constrains maximal gradient norms rather than loss values.

Based on SAM's framework [49] for minimizing sharpness, RAP [7] adapts the *zeroth-order worst-case flatness* to construct transferable adversarial examples. Motivated by RAP [7], Penalizing Gradient Norm (PGN) [8] enhances adversarial transferability by enhancing the *first-order worst-case flatness*. TPA [2] further correlates transferability with first-order average flatness (local mean gradient norms) and second-order gradient component. We give the definition of ξ -radius n -order worst-case flatness $\widehat{R}_\xi^{(n)}(\mathbf{x})$ and average-case flatness $\overline{R}_\xi^{(n)}(\mathbf{x})$ in Definition 1. Unless otherwise specified, the zeroth-order derivative is taken to be the loss function itself, i.e. $\nabla^0 J(\mathbf{x}) = J(\mathbf{x})$.

Definition 1 (ξ -radius n -order Flatness). *For any $\xi > 0$ and integer $k \in \mathbb{N}$, the worst- and average-case ξ -radius n -order flatness of the loss $J(\mathbf{x})$ at sample \mathbf{x} are defined as follows:*

- **Worst-case flatness:**

$$\widehat{R}_\xi^{(n)}(\mathbf{x}) \triangleq \max_{\mathbf{x}' \in B_\xi(\mathbf{x})} \|\nabla^n J(\mathbf{x}') - \nabla^n J(\mathbf{x})\|_2,$$

- **Average-case flatness:**

$$\overline{R}_\xi^{(n)}(\mathbf{x}) \triangleq \mathbb{E}_{\mathbf{x}' \sim \text{Unif}(B_\xi(\mathbf{x}))} [\|\nabla^n J(\mathbf{x}') - \nabla^n J(\mathbf{x})\|_2],$$

where $B_\xi(\mathbf{x}) = \{\mathbf{x}' \in \mathbb{R}^d \mid \|\mathbf{x}' - \mathbf{x}\|_\infty \leq \xi\}$ denotes the closed ℓ_∞ -ball centered at \mathbf{x} with radius ξ , $\nabla^n J(\mathbf{x})$ denotes the n -th order derivative of J at \mathbf{x} and $\text{Unif}(B_\xi(\mathbf{x}))$ denotes the uniform distribution on the set $B_\xi(\mathbf{x})$.

In Table I, we summarize six typical flatness-enhanced methods through the lens of our formalized n -order flatness metrics. Current methods adopt four distinct flatness criteria:

TABLE I

COMPARATIVE ANALYSIS OF FLATNESS-ENHANCED METHODS, SUMMARIZING THEIR CONFERENCE VENUES, OPTIMIZATION TARGET, AND FLATNESS FORMULATIONS. WE SYSTEMATICALLY COMPARE SIX REPRESENTATIVE METHODS' MATHEMATICAL FRAMEWORKS FOR ACHIEVING FLATNESS.

Flatness-Enhanced Method	Conference (Year)	Optimization Target	Flatness Formulation
Reverse Adversarial Perturbation (RAP [7])	NeurIPS 2022	$\max_{\mathbf{x}^{adv} \in B_\epsilon(\mathbf{x})} \min_{\mathbf{x}' \in B_\xi(\mathbf{x}^{adv})} J(\mathbf{x}')$	$\widehat{R}_\xi^{(0)}(\mathbf{x})$
Gradient Norm Penalty (GNP [5])	ICIP 2022	$\max_{\mathbf{x}^{adv} \in B_\epsilon(\mathbf{x})} \min_{\mathbf{x}' \in B_\xi(\mathbf{x}^{adv})} [J(\mathbf{x}^{adv}) - \lambda \cdot \ \nabla_{\mathbf{x}'} J(\mathbf{x}')\ _2]$	$\widehat{R}_\xi^{(1)}(\mathbf{x})$
Penalizing Gradient Norm (PGN [8])	NeurIPS 2023	$\max_{\mathbf{x}^{adv} \in B_\epsilon(\mathbf{x})} \min_{\mathbf{x}' \in B_\xi(\mathbf{x}^{adv})} [J(\mathbf{x}^{adv}) - \lambda \cdot \ \nabla_{\mathbf{x}'} J(\mathbf{x}')\ _2]$	$\widehat{R}_\xi^{(1)}(\mathbf{x})$
Flatness Enhanced Method (FEM [3])	ICME 2023	$\max_{\mathbf{x}^{adv} \in B_\epsilon(\mathbf{x})} \mathbb{E}_{\mathbf{x}' \sim \text{Unif } B_\xi(\mathbf{x}^{adv})} [J(\mathbf{x}')]]$	$\overline{R}_\xi^{(0)}(\mathbf{x})$
Adversarial Pixel Perturbation (APP [6])	ICIP 2023	$\max_{\mathbf{x}^{adv} \in B_\epsilon(\mathbf{x})} \mathbb{E}_{\mathbf{x}' \sim \text{Unif } B_\xi(\mathbf{x}^{adv})} [J(\mathbf{x}')]]$	$\overline{R}_\xi^{(0)}(\mathbf{x})$
Theoretically Provable Attack (TPA [2])	NeurIPS 2024	$\max_{\mathbf{x}^{adv} \in B_\epsilon(\mathbf{x})} \mathbb{E}_{\mathbf{x}' \in B_\xi(\mathbf{x}^{adv})} [\ \nabla_{\mathbf{x}'} J(\mathbf{x}')\ _2]$	$\overline{R}_\xi^{(1)}(\mathbf{x})$

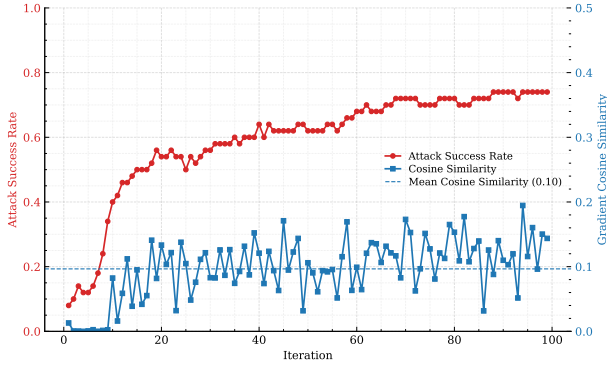
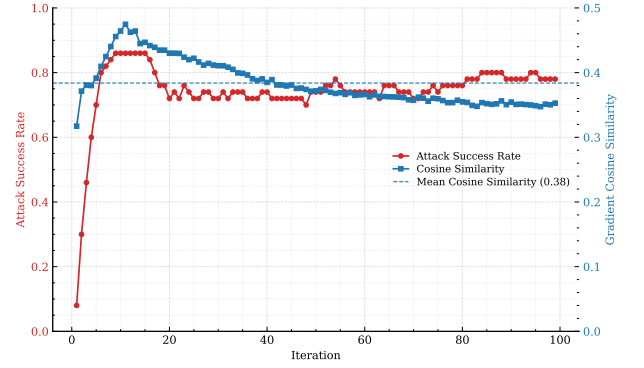
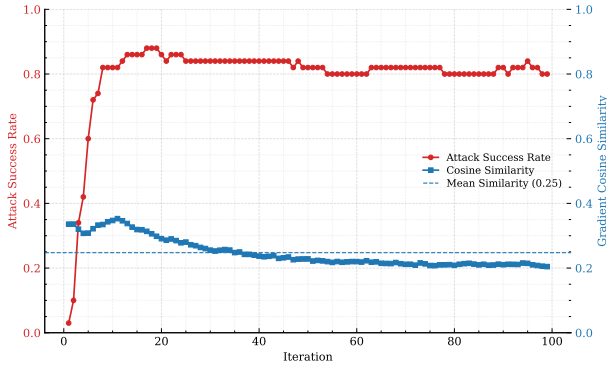
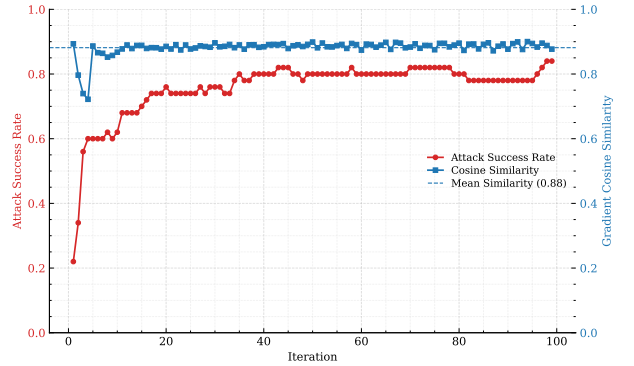
(a) RAP [7] ($\widehat{R}_\xi^{(0)}(\mathbf{x})$)(b) FEM [3] ($\overline{R}_\xi^{(0)}(\mathbf{x})$)(c) PGN [8] ($\widehat{R}_\xi^{(1)}(\mathbf{x})$)(d) TPA [2] ($\overline{R}_\xi^{(1)}(\mathbf{x})$)

Fig. 2. Optimization dynamics under flatness duality ($\overline{R}_\xi^{(n)}$ vs. $\widehat{R}_\xi^{(n)}$). Comparing zeroth/first-order methods on 100 ImageNet samples [47], we measure *inter-update* gradient similarity and transfer attack success rates (Res-50 [9]→Inc-v3 [48]). Post ASR convergence, worst-case variants sustain lower gradient similarity (0.10-0.25) than average-case ones (0.38-0.88), revealing exploration-exploitation trade-off governed by flatness formalism.

$\widehat{R}_\xi^{(0)}$, $\widehat{R}_\xi^{(1)}$, $\overline{R}_\xi^{(0)}$, and $\overline{R}_\xi^{(1)}$. While RAP [7], GNP [5], and PGN [8] optimize worst-case flatness via maximal loss ($\widehat{R}_\xi^{(0)}$) or gradient norm ($\widehat{R}_\xi^{(1)}$) constraints, FEM [3], APP [6], and TPA [2] focus on average-case objectives, either expected loss ($\overline{R}_\xi^{(0)}$) or gradient magnitudes ($\overline{R}_\xi^{(1)}$).

To our knowledge, this is the first work that unifies flatness definitions across flatness-enhanced methods and provides a taxonomy distinguishing worst/average-case flatness criteria. While prior work [52] quantifies flatness in parameter space for model robustness, our focus centers on sample-wise loss landscape flatness, a distinct perspective aligned with adversarial transferability rather than robust generalization.

B. Rethinking Flatness-Enhanced Methods

Despite the prevalent use of distinct flatness criteria, existing works neither analyze their geometric discrepancies nor characterize their inherent limitations, leading to obscured distinctions, limited performance and suboptimal efficiency. In this section, we analyze the optimization dynamics of different flatness formulation and validate the unrevealed over-exploitation and over-exploration issues in current methods.

The definition duality between average- ($\overline{R}_\xi^{(n)}$) and worst-case ($\widehat{R}_\xi^{(n)}$) flatness fundamentally governs their optimization behaviors. The expectation in $\overline{R}_\xi^{(n)}$ aggregates local gradient variations, prioritizing exploitation of dominant neigh-

borhood. While encouraging smoother updates, this gradient averaging risks over-exploitation to suboptimal plateaus dominated by local gradients. In contrast, $\widehat{R}_\xi^{(n)}$'s maximization explicitly probes extreme sensitivity points, demanding exhaustive exploration to identify maximal n -th derivative discrepancies. Such over-exploration, however, often oscillates between sensitivity peaks, particularly under practical sampling constraints, due to the non-convexity of adversarial landscapes [13], [15].

To validate the over-exploitation and over-exploration issues, we conduct an experiment on 100 ImageNet samples [47], running four flatness-enhanced methods (RAP [7], FEM [3], PGN [8], TPA [2]) for 100 iterations. We measure inter-update gradient cosine similarity during optimization on Res-50 [9] and evaluate attack success rates against Incv3 [48]. The experimental results, illustrated in Fig. 2, reveal a clear divergence. For both methods, worst-case flatness optimization exhibit significantly lower inter-iteration gradient similarities (mean similarity: RAP 0.10, PGN 0.25) compared to average-case counterparts (FEM 0.38, TPA 0.88) after convergence. The persistently low gradient similarity in worst-case optimization reveals unstable oscillation between sensitivity peaks, an indicator of over-exploration. In contrast, high similarity in average-case optimization suggests over-exploitation of local gradient consensus, leading to premature convergence on suboptimal plateaus.

Crucially, both over-exploitation and over-exploration coincide with stagnated ASR improvements, confirming our prior analysis: worst-case flatness optimization exhaustively explores non-informative sensitivity extrema, while average-case criteria over-exploit locally dominant gradient directions. These inherent limitations in both flatness criteria fundamentally constrain further enhancements to both landscape flatness and adversarial transferability, establishing a critical yet understudied challenge in balancing exploitation and exploration.

C. Design Challenges

Existing flatness-enhanced methods face two unresolved challenges: theoretical ambiguity and optimization imbalance. First, the heuristic adoption of flatness metrics lacks rigorous theoretical grounding to connect geometric flatness with adversarial transferability [7], [8], with some work even questioning their inherent correlation [2], leading to inconsistent metric selection and suboptimal performance. Second, as we shown in Section III-B, current methods suffer from a critical exploitation-exploration trade-off: average-case flatness optimization over-exploits local gradient consensus, causing premature convergence to suboptimal plateaus, while worst-case criteria induce over-exploration of non-informative sensitivity peaks, resulting in oscillatory updates. Addressing these challenges requires developing a unified framework that integrates theoretical insights into flatness-transferability relationships with adaptive mechanisms to harmonize local exploitation and global exploration, thereby maximizing adversarial transferability.

IV. THEORETICAL ANALYSIS

Building upon the systematic formalization of flatness metrics and identified challenges in Section III, this section resolves the first key challenge: the theoretical ambiguity between geometric flatness and adversarial transferability. We first establish a formal definition of transferability by introducing the adversarial loss gap, then rigorously demonstrate that improved multiple-order average-case flatness enhances adversarial transferability. This theoretical foundation directly addresses the heuristic limitations of existing methods while guiding principled optimization criteria.

A. Adversarial Transferability Formulation

To formally characterize adversarial transferability, we first define the *adversarial loss gap (ALG)* as the loss difference between adversarial and natural examples for a given model F (Definition 2). A larger ALG indicates stronger perturbation efficacy, where the adversarial example $\mathbf{x} + \delta$ significantly amplifies the model's loss compared to the original input \mathbf{x} . This metric directly quantifies how effectively δ destabilizes F 's predictions, serving as the basis for analyzing transferability.

Definition 2 (Adversarial Loss Gap). *Given a model \mathcal{F} , an input-label pair (\mathbf{x}, y) , and an adversarial perturbation δ , the adversarial loss gap (ALG) is defined as:*

$$\text{ALG}((\mathbf{x}, y), \delta; \mathcal{F}) \triangleq J(\mathbf{x} + \delta, y; \mathcal{F}) - J(\mathbf{x}, y; \mathcal{F}),$$

where J is the loss function, and $\mathbf{x} + \delta$ corresponds to the adversarial example \mathbf{x}' in (II-A).

Building on ALG, we define the dual relative and absolute transferability gaps (rATG and aATG) to quantify cross-model transferability (Definition 3). The rATG quantifies transferability by contrasting cross-model ALG differences, where positive values indicate enhanced perturbation efficacy on the target model. Based on rATG, aATG incorporates the natural loss discrepancy $J(\mathbf{x}, y; \mathcal{F}') - J(\mathbf{x}, y; \mathcal{F})$, explicitly addressing inherent model divergence on clean inputs. This makes aATG more practical for real-world scenarios where models exhibit heterogeneous behaviors even without perturbations.

Definition 3 (Relative and Absolute Transferability Gap). *Given two models \mathcal{F} and \mathcal{F}' , an input-label pair (\mathbf{x}, y) , and an adversarial perturbation δ , define*

$$\begin{aligned} \text{rATG}((\mathbf{x}, y), \delta; \mathcal{F}, \mathcal{F}') &\triangleq \text{ALG}((\mathbf{x}, y), \delta; \mathcal{F}') \\ &\quad - \text{ALG}((\mathbf{x}, y), \delta; \mathcal{F}), \end{aligned}$$

the relative adversarial transferability gap. Then the absolute adversarial transferability gap is

$$\begin{aligned} \text{aATG}((\mathbf{x}, y), \delta; \mathcal{F}, \mathcal{F}') &\triangleq \text{rATG}((\mathbf{x}, y), \delta; \mathcal{F}, \mathcal{F}') \\ &\quad + [J(\mathbf{x}, y; \mathcal{F}') - J(\mathbf{x}, y; \mathcal{F})]. \end{aligned}$$

Notably, both rATG and aATG typically yield negative values in practical attacks: while adversarial perturbations δ maximize $J(\mathbf{x} + \delta, y; \mathcal{F})$ on the surrogate model \mathcal{F} , they often induce smaller loss on \mathcal{F}' , making positive transferability gaps unrealistic. Crucially, aATG simplifies to:

$$\text{aATG}((\mathbf{x}, y), \delta; \mathcal{F}, \mathcal{F}') = J(\mathbf{x} + \delta, y; \mathcal{F}') - J(\mathbf{x} + \delta, y; \mathcal{F}).$$

When $\text{aATG} < 0$, successful transfer attacks require: minimizing $|\text{aATG}|$ to align adversarial effects across models, and maximizing $J(\mathbf{x} + \delta, y; \mathcal{F})$ to elevate the upper bound of $J(\mathbf{x} + \delta, y; \mathcal{F}')$. This joint strategy ensures sufficient adversarial impact on \mathcal{F}' despite negative gaps, formally linking to our subsequent flatness analysis.

In the next section, we will rigorously characterize the relationship between adversarial transferability and loss landscape flatness by leveraging the proposed *absolute transferability gap* (aATG) and *average-case flatness* ($\bar{R}_\xi^{(n)}$).

B. Flatness and Transferability

Based on the analysis established in Section IV-A, achieving successful adversarial transfer requires simultaneously addressing two critical objectives: (1) maximizing the adversarial loss $J(\mathbf{x} + \delta, y; \mathcal{F})$ on the surrogate model \mathcal{F} to amplify perturbation efficacy, and (2) minimizing the absolute adversarial transferability gap $|\text{aATG}|$ to align the adversarial effects between the surrogate model \mathcal{F} and the target model \mathcal{F}' . While the first objective is straightforwardly addressed through gradient-ascent-based attack methods (e.g., PGD [53]), the second objective, systematically reducing $|\text{aATG}|$, remains theoretically understudied and practically challenging. This constitutes the central focus of our theoretical analysis.

The minimization of $|\text{aATG}|$ hinges on characterizing the geometric alignment of adversarial perturbations between divergent loss landscapes. We address this by establishing a multi-order flatness-dependent bound on $|\text{aATG}|$ through Theorem 1, which directly connects transferability gaps to three measurable geometric properties: surrogate model flatness $\bar{R}_\xi^{(n)}(\mathbf{x}; F)$, Target model flatness $\bar{R}_\xi^{(n)}(\mathbf{x}; F')$, and Cross-model gradient discrepancy $C_n(\mathbf{x})$.

Theorem 1 (Flatness-based Bound on Transferability). *Let \mathcal{F} and \mathcal{F}' be two models with associated loss $J(\mathbf{x}, y; \cdot)$, and fix a point (\mathbf{x}, y) . For each integer $n \geq 0$, define*

$$C_n(\mathbf{x}) = \mathbb{E}_{\mathbf{x}' \sim \text{Unif}(B_\xi(\mathbf{x}))} \|\nabla^n J(\mathbf{x}', y; F') - \nabla^n J(\mathbf{x}', y; F)\|,$$

and let $\bar{R}_\xi^{(n)}(\mathbf{x}; F)$ and $\bar{R}_\xi^{(n)}(\mathbf{x}; F')$ be the ξ -radius n -order flatness for F and F' respectively. Then for any perturbation δ with $\|\delta\| \leq \xi$, the absolute adversarial transferability gap satisfies

$$|\text{aATG}((\mathbf{x}, y), \delta; \mathcal{F}, F')| \leq \sum_{n=0}^{\infty} \frac{\|\delta\|^n}{n!} \left[\bar{R}_\xi^{(n)}(\mathbf{x}; F) + C_n(\mathbf{x}) + \bar{R}_\xi^{(n)}(\mathbf{x}; F') \right].$$

The proof of Theorem 1 (Proof IV-B) leverages multivariate Taylor expansions to decompose aATG into infinite-order curvature alignment terms, followed by norm-based bounding of each order's contribution. This explicitly reveals how suppressing multi-order flatness variations ($n \geq 0$) and gradient discrepancies (C_n) jointly minimize transferability gaps.

Proof of Theorem 1. First, by applying the multivariate Taylor expansion of the loss around \mathbf{x} for both \mathcal{F}' and \mathcal{F} , we have

$$J(\mathbf{x} + \delta, y; F') = J(\mathbf{x}, y; F') + \sum_{n=1}^{\infty} \frac{1}{n!} \nabla_{\mathbf{x}}^n J(\mathbf{x}, y; F') [\delta^{\otimes n}],$$

$$J(\mathbf{x} + \delta, y; F) = J(\mathbf{x}, y; F) + \sum_{n=1}^{\infty} \frac{1}{n!} \nabla_{\mathbf{x}}^n J(\mathbf{x}, y; F) [\delta^{\otimes n}].$$

Subtracting these two series and including the zeroth-order term yields

$$\text{aATG}((\mathbf{x}, y), \delta; \mathcal{F}, F') = \sum_{n=0}^{\infty} \frac{1}{n!} \left(\nabla_{\mathbf{x}}^n J(\mathbf{x}, y; F') - \nabla_{\mathbf{x}}^n J(\mathbf{x}, y; F) \right) [\delta^{\otimes n}].$$

For each $n \geq 0$, set

$$T_n(\mathbf{x}) = \nabla_{\mathbf{x}}^n J(\mathbf{x}, y; F') - \nabla_{\mathbf{x}}^n J(\mathbf{x}, y; F).$$

Then for any $\mathbf{x}' \in B_\xi(\mathbf{x})$ one checks

$$T_n(\mathbf{x}) = [\nabla^n J(\mathbf{x}', y; F') - \nabla^n J(\mathbf{x}, y; F')] + [\nabla^n J(\mathbf{x}', y; F') - \nabla^n J(\mathbf{x}', y; F)] + [\nabla^n J(\mathbf{x}', y; F) - \nabla^n J(\mathbf{x}, y; F)].$$

Taking norms, applying the triangle inequality, and averaging over $\mathbf{x}' \sim B_\xi(\mathbf{x})$ gives

$$\begin{aligned} \|T_n(\mathbf{x})\| &\leq \underbrace{\mathbb{E}_{\mathbf{x}' \sim \text{Unif}(B_\xi(\mathbf{x}))} \|\nabla^n J(\mathbf{x}', y; F') - \nabla^n J(\mathbf{x}', y; F)\|}_{C_n(\mathbf{x})} \\ &\quad + \underbrace{\mathbb{E}_{\mathbf{x}' \sim \text{Unif}(B_\xi(\mathbf{x}))} \|\nabla^n J(\mathbf{x}', y; F) - \nabla^n J(\mathbf{x}, y; F)\|}_{\bar{R}_\xi^{(n)}(\mathbf{x}; F)} \\ &\quad + \underbrace{\mathbb{E}_{\mathbf{x}' \sim \text{Unif}(B_\xi(\mathbf{x}))} \|\nabla^n J(\mathbf{x}', y; F') - \nabla^n J(\mathbf{x}, y; F')\|}_{\bar{R}_\xi^{(n)}(\mathbf{x}; F')}. \end{aligned}$$

Finally, since $|T_n(\mathbf{x})[\delta^{\otimes n}]| \leq \|T_n(\mathbf{x})\| \|\delta\|^n$, we get

$$|\text{aATG}((\mathbf{x}, y), \delta; \mathcal{F}, F')| \leq \sum_{n=0}^{\infty} \frac{\|\delta\|^n}{n!} \left[\bar{R}_\xi^{(n)}(\mathbf{x}; F) + C_n(\mathbf{x}) + \bar{R}_\xi^{(n)}(\mathbf{x}; F') \right],$$

as claimed. \square

In transfer-based adversarial attacks where only the surrogate model \mathcal{F} is accessible, the controllable parameter reduces to optimizing the source flatness $\bar{R}_\xi^{(n)}(\mathbf{x}; F)$, as target model flatness $\bar{R}_\xi^{(n)}(\mathbf{x}; F')$ and cross-model discrepancy $C_n(\mathbf{x})$ remain intrinsically unmanageable. While TPA [2] attempted to theoretically link flatness and transferability, their analysis only considered first-order flatness ($n = 1$) without incorporating higher-order gradient interactions ($n \geq 2$), leading to the erroneous conclusion that flatness minimally impacts transfer performance. Our theory thus formalizes why existing flatness regularization heuristics [3], [5]–[8] succeed without target model knowledge, establishing flatness minimization on the surrogate model as both necessary and sufficient for practical transferability enhancement.

Theorem 1 also demonstrates that the impact of higher-order terms ($n \geq 1$) diminishes exponentially due to the $\frac{\|\delta\|^n}{n!}$ coefficient under ℓ_p -bounded perturbations ($\|\delta\| \ll 1$), rendering zeroth-order flatness $\bar{R}_\xi^{(0)}(\mathbf{x}; F)$, which governs expected loss variations in $B_\xi(\mathbf{x})$, the dominant contributor to transferability. This establishes zeroth-order flatness optimization as an efficient mechanism for maximizing adversarial transferability with theoretical guarantees.

V. METHOD

Building on the theoretical linkage between multi-order flatness and transferability established in Section IV, we now address the second challenge outlined in Section III-C: designing a principled mechanism to balance local exploitation and global exploration. Motivated by Theorem 1's identification of zeroth-order flatness dominance under bounded perturbations, our framework strategically focuses on optimizing $\bar{R}_\xi^{(0)}(\mathbf{x})$ through maximin expected flatness, neighborhood conditional sampling, and gradient balancing optimization to resolve the exploitation-exploration dilemma.

A. Maximin Expected Flatness

Despite the computational efficiency and desirable theoretical properties of zeroth-order flatness metrics, existing zeroth-order flatness metrics exhibit polarized limitations: worst-case flatness $\hat{R}_\xi^{(0)}(\mathbf{x})$ risks over-exploration by emphasizing local peaks, while average-case flatness $\bar{R}_\xi^{(0)}(\mathbf{x})$ tends toward over-exploitation by averaging out critical geometric features. To resolve the conflicting demands of local exploitation and global exploration in flatness optimization, we propose a novel zeroth-order worst-neighborhood average flatness metric that strategically integrates the stability of $\bar{R}_\xi^{(0)}(\mathbf{x})$ with the exploratory power of $\hat{R}_\xi^{(0)}(\mathbf{x})$.

Our key insight lies in a hierarchical decomposition of flatness measurement that first identifies high-uneven sub-regions within an expanded neighborhood, then applies average-case smoothing to stabilize gradient estimation. Formally, we define the *zeroth-order worst-neighborhood average flatness* as:

$$\hat{R}_{\gamma, \xi}^{(0)}(\mathbf{x}) \triangleq \max_{\mathbf{x}^c \in B_\gamma(\mathbf{x})} \bar{R}_\xi^{(0)}(\mathbf{x}^c),$$

where γ controls the exploration radius for identifying critical subregion centers \mathbf{x}^c , and ξ governs the neighborhood radius for zeroth-order average-case flatness computation. This hierarchical structure explicitly separates exploration scope (γ) from local smoothness (ξ), where larger γ values permit discovery of distant high-loss regions while smaller ξ values ensure stable gradient estimation within identified sub-regions.

With the proposed $\hat{R}_{\gamma, \xi}^{(0)}$, we establish the adversarial example generation framework guided by Theorem 1. As analyzed in Section IV-A, successful transfer attacks require: (i) minimizing $|\text{aATG}|$ to align adversarial effects across models, and (ii) maximizing $J(\mathbf{x} + \delta, y; \mathcal{F})$ to elevate the upper bound of target model loss $J(\mathbf{x} + \delta, y; \mathcal{F}')$. To unify

Algorithm 1 Neighborhood Conditional Sampling

Input: Surrogate model \mathcal{F} , loss function J ; a raw example \mathbf{x} with ground-truth label y ; neighborhood radius ξ , exploration radius γ ; the number of sampling points N and the max number of sampling iteration T

Output: A set of sampling points $\{\mathbf{x}_i\}_{i=1}^N$

- 1: **# Random initialization**
- 2: Initialize $\{\mathbf{x}_{0,i}\}_{i=1}^N \in U_\gamma(\mathbf{x})$
- 3: **for** $t = 0, 1, \dots, T-1$ **do**
- 4: **# Calculate the gradient of J**
- 5: $\{g_{t,i}\}_{i=1}^N = \nabla_{\mathbf{x}} J(\{\mathbf{x}_{t,i}\}_{i=1}^N, y; \mathcal{F})$
- 6: **# Update the points in sub-region**
- 7: $\{\mathbf{x}_{t+1,i}\}_{i=1}^N = \{\mathbf{x}_{t,i}\}_{i=1}^N - \xi \cdot \text{sign}(\{g_{t,i}\}_{i=1}^N)$
- 8: $\{\mathbf{x}_{t+1,i}\}_{i=1}^N = \prod_{B_\gamma(\mathbf{x})}(\prod_{B_\xi(\mathbf{x}_{0,i})}(\{\mathbf{x}_{t+1,i}\}_{i=1}^N))$
- 9: **end for**
- 10: $\{\mathbf{x}_i\}_{i=1}^N = \{\mathbf{x}_T\}_{i=1}^N$
- 11: **return** $\{\mathbf{x}_i\}_{i=1}^N$

these objectives, we formulate the attack generation as a multi-objective optimization problem:

$$\min_{\mathbf{x}^{\text{adv}} \in B_\epsilon(\mathbf{x})} \underbrace{\left[\max_{\mathbf{x}^c \in B_\gamma(\mathbf{x}^{\text{adv}})} \hat{R}_{\gamma, \xi}^{(0)}(\mathbf{x}^c) \right]}_{\text{Flatness Enhancement}} - \underbrace{J(\mathbf{x}^{\text{adv}}, y; \mathcal{F})}_{\text{Loss Maximization}}. \quad (1)$$

Substituting Definition V-A into (1) yields:

$$\min_{\mathbf{x}^{\text{adv}} \in B_\epsilon(\mathbf{x})} \left\{ \max_{\mathbf{x}^c \in B_\gamma(\mathbf{x}^{\text{adv}})} \mathbb{E}_{\mathbf{x}' \sim \text{Unif}(B_\xi(\mathbf{x}^c))} [|J(\mathbf{x}') - J(\mathbf{x}^c)|] - J(\mathbf{x}^{\text{adv}}) \right\}. \quad (2)$$

Under the ℓ_∞ -norm perturbation constraint $\|\mathbf{x}' - \mathbf{x}^c\|_\infty \leq \xi$, $\|\mathbf{x}^{\text{adv}} - \mathbf{x}^c\|_\infty \leq \gamma$, we observe:

$$J(\mathbf{x}^{\text{adv}}) - J(\mathbf{x}^c) \approx 0, J(\mathbf{x}') - J(\mathbf{x}^c) \leq 0. \quad (3)$$

Substituting (3) into (2), we derive the final optimization objective:

$$\max_{\mathbf{x}^{\text{adv}} \in B_\epsilon(\mathbf{x})} \min_{\mathbf{x}^c \in B_\gamma(\mathbf{x}^{\text{adv}})} \mathbb{E}_{\mathbf{x}' \sim \text{Unif}(B_\xi(\mathbf{x}^c))} J(\mathbf{x}'), \quad (4)$$

where the expectation term $\mathbb{E}[J(\mathbf{x}')]$ represents the *expected flatness* over local neighborhoods. This maximin structure motivates our method's name: **Maximin Expected Flatness (MEF)**, which strategically explores worst-case neighborhoods while exploiting average loss landscapes.

B. Neighborhood Conditional Sampling

Directly solving the inner minimization in (4) is computationally infeasible due to the continuous loss landscape and infinite candidates in $B_\gamma(\mathbf{x}^{\text{adv}})$. To efficiently approximate this intractable problem and obtain representative sampling points capturing worst-case flatness, we propose **Neighborhood Conditional Sampling (NCS)** method that leverages gradients for guided exploration.

The NCS begins by uniformly sampling N points $\{\mathbf{x}_{0,i}\}_{i=1}^N$ within $B_\xi(\mathbf{x})$. At each iteration t , gradients $\nabla_{\mathbf{x}} J(\mathbf{x}_{t,i}, y; \mathcal{F})$ are computed for all points, followed by a sign-based update:

$$\mathbf{x}_{t+1,i} = \mathbf{x}_{t,i} - \xi \cdot \text{sign}(\nabla_{\mathbf{x}} J(\mathbf{x}_{t,i}, y; \mathcal{F})),$$

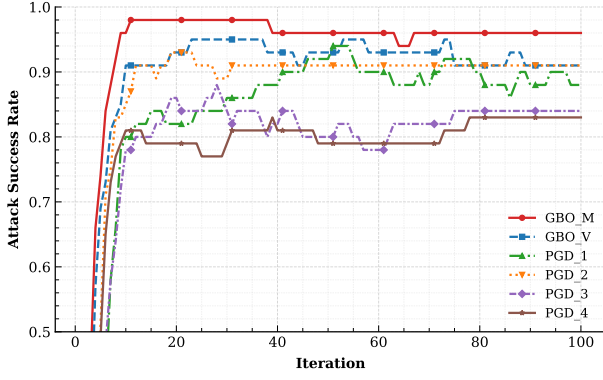


Fig. 3. GBO’s dual optimization superiority in transferability (Res-50 [9]→Inc-v3 [48]). Achieving 90-98% transfer attack success rates within 10 iterations, GBO outperforms PGD’s 84-90% at 100 steps with 6-14% absolute improvement, while attaining 10× faster convergence on 100 ImageNet samples.

which prioritizes directional consistency over gradient magnitudes. Updated points are then projected back to $B_\xi(\mathbf{x}_{0,i})$ and $B_\gamma(\mathbf{x})$ to enforce spatial constraints. After T iterations, the final set $\{\mathbf{x}_{T,i}\}_{i=1}^N$ captures regions with minimal expected loss. This approach (summarized in Algorithm 1) eliminates sampling overhead by leveraging gradients, reducing computation costs while maintaining efficiency.

C. Gradient Balancing Optimization

The nested maximin structure in (4) introduces an imbalanced optimization challenge: the inner minimization requires fine-grained gradient descent across N sampling points, while the outer maximization must update a single adversarial example \mathbf{x}^{adv} to elevate losses globally. This asymmetry arises because precise inner updates demand multiple iterations, whereas the outer optimization struggles to coordinate perturbations that simultaneously affect all minimized sub-regions. Experiments with gradient descent (1–4 inner steps) on 100 ImageNet images (Res-50→Inc-v3) validate the issue: stricter inner optimization drastically increases required convergence steps while reducing transfer attack success rates (Figure 3), confirming the inherent imbalance.

To address the imbalanced maximin optimization problem, we propose **Gradient Balancing Optimization (GBO)**, which strategically weakens the inner minimization’s dominance by reusing outer maximization gradients. Let $\{g_{t,i}\}_{i=1}^N = \nabla_{\mathbf{x}} J(\{\mathbf{x}'_{t,i}\}_{i=1}^N, y; \mathcal{F})$ denote the gradients from the outer maximization at iteration t . Instead of computing separate gradients for inner minimization, GBO approximates them as:

$$\nabla_{\mathbf{x}'_{t,i}} J(\mathbf{x}'_{t,i}, y; \mathcal{F}) \approx g_{t-1,i},$$

leveraging the geometric proximity between consecutive adversarial examples. This shared gradient scheme entirely eliminates the computational overhead of inner minimization by reusing outer gradients for inner updates, accelerates convergence through aligned optimization directions, and improves transfer attack success rates.

Algorithm 2 Maximin Expected Flatness (MEF) Attack

Input: Surrogate model \mathcal{F} and the loss function J ; A raw example \mathbf{x} with ground-truth label y ; The perturbation magnitude ϵ ; the maximum iterations T ; the outer/inner decay factor μ_{outer}/μ_{inner} ; the number of randomly sampled examples, N ; neighborhood radius ξ , exploration radius γ .

Output: An adversarial example \mathbf{x}^{adv}

- 1: $g_0^{outer} = 0$; $\{g_{0,i}^{inner}\}_{i=1}^N = 0$; $\mathbf{x}_0^{adv} = \mathbf{x}$; $\alpha = \epsilon/T$
- 2: **for** $t = 0, 1, \dots, T-1$ **do**
- 3: **# Neighborhood Conditional Sampling**
- 4: $\{\mathbf{x}_{t,i}\}_{i=1}^N \in U_\gamma(\mathbf{x}_t^{adv})$
- 5: $\{\mathbf{x}'_{t,i}\}_{i=1}^N = \{\mathbf{x}_{t,i}\}_{i=1}^N + \xi \cdot \text{sign}(\{g_{t,i}^{inner}\}_{i=1}^N)$
- 6: **# Gradient Calculation**
- 7: $\{g_{t,i}\}_{i=1}^N = \nabla_{\mathbf{x}} J(\{\mathbf{x}'_{t,i}\}_{i=1}^N, y; \mathcal{F})$
- 8: **# Gradient Balancing Optimization**
- 9: $\{g_{t,i}^{inner}\}_{i=1}^N = \frac{\{g_{t,i}\}_{i=1}^N}{\|\{g_{t,i}\}_{i=1}^N\|_1} - \mu_{inner} \cdot \{g_{t,i}^{inner}\}_{i=1}^N$
- 10: **# Outer Gradient Update**
- 11: $g_t^{outer} = \mu_{outer} \cdot g_t^{outer} + \frac{1}{N} \sum_{i=1}^N \frac{\{g_{t,i}\}_{i=1}^N}{\|\{g_{t,i}\}_{i=1}^N\|_1}$
- 12: **# Adversarial Example Update**
- 13: $\mathbf{x}_{t+1}^{adv} = \Pi_{B_\epsilon(\mathbf{x})}[\mathbf{x}_t^{adv} + \alpha \cdot \text{sign}(g_t^{outer})]$
- 14: **end for**
- 15: **return** \mathbf{x}_T^{adv} .

To stabilize gradient directions, we further introduce momentum:

$$\{g_{t,i}^{inner}\}_{i=1}^N = \frac{\{g_{t,i}\}_{i=1}^N}{\|\{g_{t,i}\}_{i=1}^N\|_1} - \mu_{inner} \cdot \{g_{t,i}^{inner}\}_{i=1}^N,$$

where μ_{inner} controls historical gradient contributions. We compare GBO_M (momentum-enhanced) and GBO_V (vanilla) against PGD-based inner minimization with different iteration steps (1–4) on 100 ImageNet images. As shown in Fig. 3, GBO achieves faster convergence and higher transfer success rates than gradient-intensive PGD baselines, with GBO_M (momentum-enhanced) outperforming GBO_V (vanilla) in attack success rates. This demonstrates that gradient reuse with momentum stabilization not only resolves the optimization imbalance but also maximizes transferability, making GBO_M our default solution.

D. Algorithm

The proposed framework integrates the objective of **Maximin Expected Flatness**, **Neighborhood Conditional Sampling**, and **Gradient Balancing Optimization** through a unified max-min bi-level algorithm summarized in Algorithm 2. The outer loop maximizes the expected flatness over adversarially identified critical sub-regions, while the inner loop approximates worst-case neighborhoods via gradient-guided sampling with momentum-stabilized direction reuse. By strategically sharing normalized gradients between inner minimization and outer maximization, the algorithm achieves an optimal balance between computational efficiency and attack effectiveness.

TABLE II

TRANSFER ATTACK SUCCESS RATE (%) COMPARISON OF GRADIENT-STABILIZED ATTACKS ON NORMALLY TRAINED MODELS. EVALUATED ACROSS FOUR SURROGATE MODELS AND EIGHT DIVERSE TARGET ARCHITECTURES, OUR MEF_H AND MEF_F VARIANTS CONSISTENTLY OUTPERFORM 12 EXISTING METHODS IN ATTACK PERFORMANCE. THE BEST RESULTS ARE BOLD AND THE SECOND BEST RESULTS ARE UNDERLINED.

Attack	Res-50 \Rightarrow							Res-101 \Rightarrow						
	Res-101	Inc-v3	Inc-v4	IncRes-v2	VGG-19	Dense-121	Xcept	Res-50	Inc-v3	Inc-v4	IncRes-v2	VGG-19	Dense-121	Xcept
MI [21]	93.3	50.5	46.0	31.8	79.1	86.1	53.3	94.4	50.6	43.9	33.7	73.4	82.2	51.8
NI [22]	96.7	56.5	49.1	35.9	84.0	88.5	56.4	97.8	55.2	50.9	37.8	79.0	85.8	55.0
PI [4]	98.0	60.2	54.4	38.1	88.1	92.8	60.7	98.5	62.4	55.9	42.2	83.4	90.7	60.2
TPA [2]	96.2	60.5	55.0	40.4	85.9	90.5	60.7	97.2	58.1	54.2	43.2	81.4	88.8	60.9
GNP [5]	98.7	69.8	64.7	50.6	91.7	95.7	68.2	99.1	70.3	64.5	52.0	87.9	93.9	68.5
VMI [1]	98.2	72.8	68.6	57.4	91.3	95.7	73.2	98.6	73.2	68.4	57.6	88.5	93.6	70.5
VNI [1]	98.8	77.2	73.4	61.6	93.7	96.8	75.7	99.4	77.4	73.1	62.8	91.3	95.4	75.0
EMI [4]	99.3	75.0	71.2	54.3	94.8	97.2	74.3	99.8	76.8	72.6	58.5	92.9	97.2	74.0
RAP [7]	97.8	70.2	65.9	50.6	91.3	94.3	70.9	98.7	70.1	65.1	52.1	89.3	93.3	70.2
APP [6]	99.3	83.1	79.6	73.1	95.3	97.8	83.3	99.4	83.2	80.9	72.8	93.4	96.6	82.0
FEM [3]	<u>99.8</u>	89.4	86.3	78.8	97.4	98.7	87.7	<u>99.8</u>	89.1	86.4	77.6	95.4	98.0	87.3
PGN [8]	99.2	86.3	83.9	79.0	95.6	97.8	86.9	99.5	86.8	84.5	80.0	94.5	97.1	88.1
MEF _H	99.7	<u>90.6</u>	<u>88.7</u>	<u>82.7</u>	<u>98.3</u>	<u>99.4</u>	<u>90.4</u>	99.7	<u>91.2</u>	<u>88.2</u>	<u>82.2</u>	<u>97.0</u>	<u>98.4</u>	<u>90.0</u>
MEF _F	99.9	95.1	94.2	91.3	99.2	99.8	94.7	99.9	95.8	95.2	91.8	98.9	99.4	95.7

Attack	Inc-v3 \Rightarrow							Inc-v4 \Rightarrow						
	Res-50	Res-101	Inc-v4	IncRes-v2	VGG-19	Dense-121	Xcept	Res-50	Res-101	Inc-v3	IncRes-v2	VGG-19	Dense-121	Xcept
MI [21]	54.6	48.8	51.2	43.3	56.0	55.7	56.1	56.1	51.3	58.2	43.3	61.7	58.3	56.8
NI [22]	63.8	58.0	61.3	53.3	63.7	64.3	62.5	62.3	56.7	65.5	49.7	68.9	64.2	64.2
PI [4]	66.1	60.7	64.3	56.8	65.6	67.7	64.9	64.3	59.9	69.8	54.0	71.9	68.3	66.6
TPA [2]	59.4	54.2	60.4	54.2	64.3	60.9	64.7	61.6	53.3	66.7	56.1	70.7	64.2	72.0
GNP [5]	60.5	55.1	65.9	56.0	64.7	61.5	66.3	58.3	51.9	64.6	56.6	66.4	60.0	71.2
VMI [1]	69.6	65.4	71.3	64.7	70.9	72.0	71.8	70.7	66.6	77.6	66.8	76.3	74.6	73.0
VNI [1]	76.1	71.2	76.9	71.3	75.7	77.7	76.4	75.3	71.4	82.1	71.0	80.8	77.9	77.4
EMI [4]	78.8	74.3	78.5	72.2	79.5	80.5	78.6	79.0	75.3	86.5	71.9	85.4	82.1	82.7
RAP [7]	81.3	74.2	75.4	67.7	80.7	79.5	78.1	81.9	76.9	82.1	65.5	87.9	82.4	82.3
APP [6]	73.5	68.0	79.2	73.1	74.7	75.7	78.5	69.0	64.7	77.1	73.5	74.7	72.5	80.7
FEM [3]	82.1	77.1	87.2	82.1	81.8	82.1	84.5	78.3	73.9	86.0	78.9	81.6	80.4	86.9
PGN [8]	84.6	79.9	88.4	84.9	84.6	86.9	89.1	84.9	82.3	91.1	85.8	89.0	87.6	90.8
MEF _H	<u>85.8</u>	<u>80.8</u>	<u>89.4</u>	<u>86.1</u>	<u>85.2</u>	<u>87.4</u>	<u>89.9</u>	<u>86.2</u>	<u>82.4</u>	<u>92.8</u>	<u>86.1</u>	<u>90.1</u>	<u>88.5</u>	<u>90.8</u>
MEF _F	92.6	91.5	96.5	94.3	92.8	93.4	95.8	91.4	90.3	94.5	91.2	92.2	91.9	95.1

VI. EXPERIMENTS

A. Experimental Setup

Dataset. We conduct experiments on the ImageNet-compatible dataset consisting of 1,000 images (299×299 resolution with annotated labels), which serves as the standard benchmark in previous works [7], [8], [31], [54]–[56].

Models. We select Inception-v3 (Inc-v3) [48], Inception-v4 (Inc-v4) [57], ResNet-50 (Res-50) [9] and ResNet-101 (Res-101) [9] with TorchVision-pretrained weights [58] for generating adversarial examples. Transferability evaluation covers: (1) *Standard CNNs*: Inc-v3 [48], Inc-v4 [57], Res-50 [9], Res-101 [9], Inception-ResNetv2 (IncRes-v2) [57], DenseNet-121 (Dense-121) [59], VGG-19bn (VGG-19) [60] and Xception (xcept) [61]; (2) *Cross-architectures*: MobileNet-v2 (MobileNet) [62], PNASNet-5-Large (PNASNet-L) [63], ViT-Base/16 (ViT-B/16) [64], ViT-Large/32 (ViT-L/32) [64], PiT-S [65], MLP-Mixer [66] and ResMLP [67]; (3) *Defended models*: Adversarially trained Inc-v3_{adv} [37], Inc-v3_{ens3} [38], Inc-v3_{ens4} [38] and IncRes-v2_{ens} [38]; adversarial purification defenses HGD [41] and NRP [43]; certifiable defense RS [39].

Compared Methods. We evaluate against 24 transfer-based adversarial attacks spanning three categories: (1) 5 *data-driven methods* covering input augmentation (DI [19], TI [20], SI [22], Admix [25], SSA [26]); (2) 4 *model-driven methods* comprising model ensemble (SVRE [31], CWA [32]) and surrogate refinement (SGM [30], LinBP [23]) strategies; (3) 15 *optimization-driven methods* including feature-based

(ILA [35], NAA [24]), generative (CDA [36]), gradient stabilization (MI [21], NI [22], PI/EMI [4], VMI/VNI [1]), and flatness-enhanced (RAP [7], PGN [8], GNP [5], FEM [3], APP [6], TPA [2]) approaches. PGN [8] constitutes the state-of-the-art in optimization-driven methods.

Hyper-parameters. All baseline methods use their originally reported optimal configurations unless specified. We unify common parameters across attacks: maximum perturbation $\epsilon = 16/255$, iteration $T = 10$, and step size $\alpha = \epsilon/T$. Sampling-based attacks employ $N = 20$ samples for enhanced gradient estimation, double the typical setting in prior works. Specialized parameters retain original setups: RAP [7] uses $\alpha = 1.6/255$ with $K = 400$ iterations ($K_{LS} = 100$ for late-start phase). Our MEF sets neighborhood radius $\gamma = 2 \times \epsilon$, exploration radius $\xi = 0.15 \times \epsilon$, outer/inner momentum coefficient $\mu_{outer}/\mu_{inner} = 0.5/0.9$. Our MEF requires only one backpropagation per sample versus PGN (current SOTA)’s two. For comprehensive evaluation, we design two variants: MEF_H (10 iterations, half PGN’s cost) and MEF_F (20 iterations, fully matching PGN’s cost).

Evaluation Framework. In our experiment, adversarial examples generated on white-box surrogates are directly transferred to black-box targets for transfer attack success rate evaluation, with systematic analysis across three dimensions: (1) *target model attributes* spanning standard CNNs (Sec. VI-B), defended models (Sec. VI-C), and cross-architecture variants (Supp. Sec. A), demonstrating attack generalization across

TABLE III

TRANSFER ATTACK SUCCESS RATE (%) AGAINST MODERN DEFENSE MECHANISMS. EVALUATING ACROSS THREE DEFENSE CATEGORIES ON SEVEN PROTECTED TARGETS. THE BEST RESULTS ARE BOLD AND THE SECOND BEST RESULTS ARE UNDERLINED.

Attack	Res-50 \Rightarrow							Inc-v3 \Rightarrow						
	Inc-v3 _{adv}	Inc-v3 _{ens3}	Inc-v3 _{ens4}	IncRes-v2 _{ens}	RS	HGD	NRP	Inc-v3 _{adv}	Inc-v3 _{ens3}	Inc-v3 _{ens4}	IncRes-v2 _{ens}	RS	HGD	NRP
MI [21]	21.6	17.2	16.4	9.4	25.6	19.4	53.5	27.3	22.4	23.3	11.2	24.5	8.9	30.7
NI [22]	21.8	18.3	17.3	9.2	25.7	17.0	55.4	27.8	22.8	22.6	11.1	24.4	8.4	30.5
PI [4]	22.7	19.1	17.5	9.8	26.6	21.6	60.7	30.9	24.5	24.3	12.6	24.7	9.8	30.9
TPA [2]	25.7	18.1	15.5	9.3	28.4	6.7	58.2	27.8	18.0	16.2	8.6	25.8	2.3	33.2
GNP [5]	29.2	24.8	23.2	13.3	28.1	26.5	70.7	30.5	24.0	23.5	11.7	25.1	6.5	34.4
VMI [1]	36.5	35.4	34.3	21.8	30.6	45.8	73.7	45.3	41.2	41.6	25.1	27.3	24.5	38.5
VNI [1]	37.8	35.5	34.7	23.8	30.9	47.4	75.9	47.8	44.4	43.9	26.8	28.0	26.7	38.9
EMI [4]	29.5	23.6	22.4	12.5	29.0	28.9	71.4	39.8	33.5	31.4	17.7	27.2	13.5	38.3
RAP [7]	29.4	17.4	16.9	8.8	32.1	4.0	63.2	32.2	16.3	16.2	7.9	27.3	1.5	27.6
APP [6]	51.1	50.0	49.5	35.6	39.6	61.3	89.0	53.7	47.2	47.3	29.9	31.4	24.1	44.2
FEM [3]	50.2	49.3	46.4	31.4	36.4	72.2	89.5	56.2	49.7	49.4	28.5	29.9	23.5	43.0
PGN [8]	60.2	58.4	59.6	45.6	48.1	62.5	92.9	69.2	61.1	62.2	41.6	38.1	27.7	54.6
MEF _H	<u>62.4</u>	<u>64.5</u>	<u>63.3</u>	<u>50.4</u>	<u>49.2</u>	<u>80.6</u>	<u>94.6</u>	<u>69.7</u>	<u>65.1</u>	<u>65.4</u>	<u>45.4</u>	<u>38.3</u>	<u>46.3</u>	<u>54.8</u>
MEF _F	70.1	69.2	65.1	52.2	51.5	83.0	97.2	75.8	69.0	69.6	47.9	40.4	52.4	56.2

TABLE IV

TRANSFER ATTACK SUCCESS RATE (%) COMPARISON WITH INPUT AUGMENTATION ATTACKS. USING RES-50 AND INC-V3 AS SURROGATES, MEF_{H/F} VARIANTS OUTPERFORM FIVE INPUT AUGMENTATION BASELINES ACROSS SIX TARGETS WHILE USING LESS COMPUTATION. THE BEST RESULTS ARE BOLD AND THE SECOND BEST RESULTS ARE UNDERLINED.

Attack	Res-50 \Rightarrow						Inc-v3 \Rightarrow					
	IncRes-v2	Inc-v3 _{ens3}	Inc-v4 _{ens4}	IncRes-v2 _{ens}	ViT-L/32	MLP-Mixer	IncRes-v2	Inc-v3 _{ens3}	Inc-v4 _{ens4}	IncRes-v2 _{ens}	ViT-L/32	MLP-Mixer
DI [19]	70.2	37.5	36.5	23.1	29.5	59.2	66.7	37.1	35.7	18.8	26.3	54.3
MEF _H +DI	89.7	<u>77.5</u>	<u>76.1</u>	<u>66.1</u>	<u>50.3</u>	<u>74.5</u>	88.3	74.8	74.7	56.2	41.6	67.8
MEF _F +DI	95.3	83.8	80.5	68.6	55.1	79.8	94.2	78.0	77.6	58.0	46.4	74.1
TI [20]	51.1	42.0	39.1	30.2	34.4	55.6	52.0	37.0	37.2	26.0	28.8	53.7
MEF _H +TI	81.7	<u>77.4</u>	<u>77.8</u>	<u>68.2</u>	<u>57.3</u>	<u>71.1</u>	86.4	79.6	79.5	67.4	48.7	68.3
MEF _F +TI	94.1	83.5	82.6	73.6	62.5	76.0	94.5	89.0	88.3	78.8	56.3	75.6
SI [22]	56.8	29.6	29.5	17.4	24.9	49.5	65.2	34.7	35.3	18.3	25.1	53.7
MEF _H +SI	86.9	71.3	69.7	56.8	<u>44.1</u>	67.1	89.4	<u>75.7</u>	<u>75.0</u>	<u>55.2</u>	<u>39.4</u>	<u>64.2</u>
MEF _F +SI	92.8	78.6	74.7	61.2	48.8	73.0	95.9	81.7	80.5	57.8	44.9	72.2
Admix [25]	52.5	23.6	22.2	13.1	23.9	50.4	64.2	29.7	27.7	14.7	23.6	52.8
MEF _H +Admix	70.5	<u>39.2</u>	<u>37.0</u>	<u>24.5</u>	<u>27.0</u>	<u>55.5</u>	<u>83.5</u>	<u>45.3</u>	<u>45.8</u>	<u>27.1</u>	<u>26.5</u>	<u>56.5</u>
MEF _F +Admix	86.4	46.6	42.1	27.7	31.6	64.1	94.7	51.1	51.9	30.1	31.0	67.6
SSA [26]	83.0	50.2	47.3	31.3	<u>35.6</u>	64.7	83.7	52.4	54.7	31.0	<u>33.3</u>	62.3
MEF _H +SSA	81.6	<u>53.9</u>	<u>51.1</u>	<u>38.0</u>	33.0	61.1	<u>84.4</u>	<u>54.9</u>	<u>56.3</u>	<u>34.2</u>	30.9	58.2
MEF _F +SSA	90.1	58.1	53.5	39.0	35.7	68.0	92.2	58.2	60.3	35.1	35.3	65.7
MEF _H	83.7	64.5	63.3	50.4	40.8	65.3	86.1	65.1	65.4	45.4	35.2	65.5
MEF _F	90.3	69.2	65.1	52.2	44.9	71.7	94.3	69.0	69.6	47.9	40.3	69.4

model architectures and defense mechanisms; (2) *methodological categories* comparing ensemble (Supp. Sec. B), data-driven augmentation (Sec. VI-D), and feature/generative/surrogate attacks (Sec. VI-E), highlighting superiority over existing attack paradigms; (3) *method-intrinsic analysis* evaluating parametric sensitivity (γ/ξ , μ_{outer}/μ_{inner} , N/T in Sec. VI-F), and loss landscape via flatness measurements versus current flatness-enhanced methods (Supp. Sec. C), validating parameter robustness and flatness gains in loss landscape.

B. Evaluation on Normally Trained Models

We evaluate our MEF_H and MEF_F attacks against 12 representative gradient stabilization methods on normally trained models. For each baseline, we generate adversarial examples on four standard source models (Res-50 [9], Res-101 [9], Inc-v3 [48], and Inc-v4 [57]), then measure attack success rates across eight diverse target models: Inc-v3 [48], Inc-v4 [57], Res-50 [9], Res-101 [9], IncRes-v2 [57], Dense-121 [59], VGG-19 [60], and Xception [61].

As shown in Table II, both MEF variants significantly outperform existing methods. Notably, MEF_H achieves an average attack success rate of 89.93% across all targets while requiring only half the computational budget of PGN [8]. This

surpasses PGN's 88.18% average success rate despite using 50% fewer backpropagation steps. When matching PGN's computational cost, MEF_F elevates the average success rate to 94.84%, a 6.66% absolute improvement over PGN. Remarkably, MEF_F maintains over 90% success rates on every individual target model, demonstrating unprecedented cross-model transferability. These results establish that our MEF attack effectively balances efficiency and attack performance, achieving new SOTA transferability under both half-cost and full-cost settings.

C. Evaluation on Defended Models

To evaluate robustness against modern defenses, we generate adversarial examples on Inc-v3 [48] and Res-50 [9] source models, then transfer them to seven protected targets: (1) adversarially trained models (Inc-v3_{adv} [37], Inc-v3_{ens3} [38], Inc-v3_{ens4} [38], IncRes-v2_{ens} [38]), (2) purification defenses (HGD [41], NRP [43]), and (3) certifiable adversarial defense RS [39]. For NRP [43], we evaluate attack success rates on Res-101 [9] after applying its purification process.

Table III compares MEF_H/MEF_F with 12 gradient stabilization attacks. MEF_H achieves 59.87% average success rate across all defenses using half the computational budget of

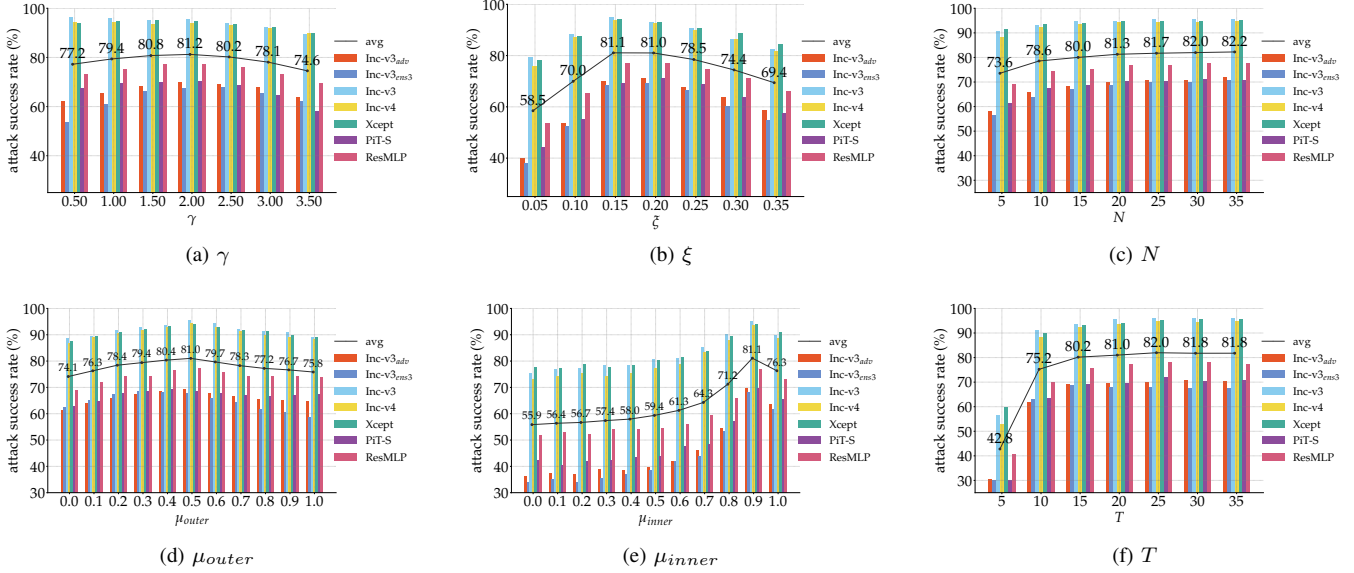


Fig. 4. Parameter ablation study on MEF, evaluating γ/ξ , μ_{inner}/μ_{outer} , and N/T impacts on transfer success rates across six challenging targets (Inc-v3 [48], Inc-v4 [57], Xception [61], PiT-S [65], ResMLP [67], Inc-v3_{adv} [37] and Inc-v3_{ens3} [38]).

PGN [8], surpassing PGN’s 55.84% baseline. When matching PGN’s cost, MEF_F further elevates the average success rate to 62.89%, a 7.05% absolute improvement. Notably, MEF_F outperforms all competitors on individual defense types: 7.63% against adversarial training, 12.73% over purification defenses, and 4.1% versus RS certification. This consistent superiority demonstrates our method’s capability to bypass diverse defense mechanisms, establishing new state-of-the-art robustness against protected models.

D. Integrated with Input Augmentation Attacks

We compare MEF_H and MEF_F against five input augmentation attacks: DI [19], TI [20], SI [22], Admix [25], and SSA [26]. Adversarial examples are generated on Res-50 [9] and Inc-v3 [48], then transferred to six challenging targets: IncRes-v2 [57], Inc-v3_{ens3} [38], Inc-v4_{ens4} [38], IncRes-v2_{ens} [38], ViT-L/32 [64], and MLP-Mixer [66]. For fair comparison, each input augmentation attack uses 40 augmented copies per iteration (total $T = 10$), requiring 40 back-propagations per step. This makes MEF_H (10 iterations, 20 samples) half as costly as input augmentation baselines, while MEF_F (20 iterations, 20 samples) matches their computational budget. We further integrate sample transformations from input augmentation methods into MEF variants without introducing additional gradient computations.

Table IV reveals two key findings: (1) MEF_H achieves superior transferability (55.12% average success rate) with 50% less computational cost than input augmentation baselines (52.46% for best baseline SSA [26]). When matching the budget, MEF_F outperforms SSA by 12.87% (65.33% vs. 52.46%); (2) Combining MEF with input transformations yields substantial gains. For instance, MEF_F+TI attains 79.57% average success rate without extra computation, surpassing SSA [26] by 27.11%. This demonstrates that our gradient stabilization framework synergizes effectively with input transformations, particularly benefiting from TI’s translation-invariant patterns.

These results validate that MEF provides a more efficient and effective approach than pure input augmentation strategies for enhancing transferability.

TABLE V
TRANSFER ATTACK SUCCESS RATE (%) COMPARISON ACROSS ATTACK PARADIGMS. THE BEST RESULTS ARE BOLD AND THE SECOND BEST RESULTS ARE UNDERLINED.

Attack	Inc-v3	Inc-v4	Res-101	Inc-v3 _{ens3}	Inc-v3 _{ens4}	IncRes-v2 _{ens}	AVG
SGM [30]	71.6	35.3	92.8	12.3	12.5	6.1	38.4
LinBP [23]	72.7	47.9	95.4	13.2	13.3	6.8	41.6
ILA [35]	70.5	74.8	97.9	16.5	15.3	9.0	47.3
NAA [24]	82.7	82.4	98.3	30.1	29.6	21.0	57.4
CDA [36]	69.4	83.1	94.5	49.8	52.7	43.3	65.5
MEF _H	<u>90.6</u>	<u>88.7</u>	<u>99.7</u>	<u>64.5</u>	<u>63.3</u>	<u>50.4</u>	<u>76.2</u>
MEF _F	95.1	94.2	99.9	69.2	65.1	52.2	79.3

E. Comparison with Other Types of Attacks

We further validate MEF’s generality by comparing it with three distinct attack paradigms: (1) *surrogate refinement* methods (SGM [30], LinBP [23]), (2) *feature-based* approaches (ILA [35], NAA [24]), and (3) *generative modeling* attack CDA [36]. To ensure fair comparison, all methods generate adversarial examples on Res-50 [9], the prerequisite architecture for LinBP’s skip connection optimization.

As shown in Table V, MEF_H achieves 76.2% average success rate across six target models (Inc-v3 [48], Inc-v4 [57], Res-101 [9], Inc-v3_{ens3} [38], Inc-v3_{ens4} [38] and IncRes-v2_{ens} [38]), surpassing CDA [36] (65.5%) by 10.7%. Notably, MEF_F elevates performance to 79.3%, outperforming CDA [36] (65.5%) by 13.8%. These results demonstrate that our framework consistently outperforms attacks relying on model-specific refinement, intermediate feature alignment, or generative priors.

F. Ablation Study

To analyze the impact of key components in MEF, we conduct parametric sensitivity studies on six critical parameters: neighborhood radius γ , exploration radius ξ , outer/inner

momentum coefficients (μ_{outer} , μ_{inner}), sampling size N , and iteration count T . Each parameter's influence on transferability is evaluated by systematically varying its value while fixing others to default configurations (pre-optimized via exhaustive subset search). Adversarial examples generated on Res-50 are transferred to seven challenging targets spanning standard models (Inc-v3 [48], Inc-v4 [57], Xception [61]), cross-architectures (PiT-S [65], ResMLP [67]), and defended models (Inc-v3_{adv} [37], Inc-v3_{ens3}) [38], providing comprehensive insights into parameter robustness across diverse scenarios.

Figure 4 reveals three critical trends. First, both neighborhood radius γ and exploration radius ξ (scaled by ϵ) exhibit optimal mid-range values: $\gamma = 2\epsilon$ and $\xi = 0.15\epsilon$ maximize transferability. Notably, ξ demonstrates higher sensitivity than γ , yet both optimal values generalize consistently across all targets. Second, while outer momentum $\mu_{outer} = 0.5$ provides marginal gains, inner momentum $\mu_{inner} = 0.9$ proves indispensable, delivering a 10% success rate boost by balancing historical and current gradient contributions. Third, increasing sampling size N from 5 to 20 improves performance by 6.4%, with diminishing returns beyond $N = 15$, while extending iterations T from 5 to 20 yields 37.2% gains before stabilizing. To balance efficiency and performance, we design MEF_H (10 iterations, half PGN [8]'s computational cost) and MEF_F (20 iterations, matching PGN [8]'s full cost). These results validate that MEF achieves superior transferability through geometry-aware gradient stabilization rather than brute-force sampling or excessive iterations.

VII. CONCLUSION

This work establishes the first theoretical foundation linking multi-order flatness enhancement to adversarial transferability, and proposes a novel flatness-based adversarial attack framework that achieves state-of-the-art transferability performance. In specific, we systematically unify fragmented flatness definitions across existing flatness-enhanced methods, revealing their inconsistent metric adoption and inherent limitations in over-exploration of sensitivity peaks or over-exploitation of local gradients. To resolve these issues, we rigorously formalize the geometric relationship between average-case flatness and transferability gaps, proving that enhancing multi-order average-case flatness minimizes cross-model discrepancies. Based on this theory, we design a maximin expected flatness (MEF) attack that balances worst-neighborhood exploration and local averaging, along with effective sampling methods (NCS) and efficient optimization strategies (GBO) to harmonize gradient exploitation and exploration. Extensive experiments across 22 diverse models and comparisons with 24 state-of-the-art transfer-based attack methods demonstrate our framework's superior attack success rates and faster computational efficiency than existing approaches. We anticipate this work will inspire broader adoption of flatness principles in AI security and safety research, particularly for enhancing adversarial robustness evaluation and designing next-generation adversarial defense mechanisms.

REFERENCES

- [1] X. Wang and K. He, "Enhancing the transferability of adversarial attacks through variance tuning," in *Proceedings of the IEEE/CVF conference on computer vision and pattern recognition*, 2021, pp. 1924–1933.
- [2] M. Fan, X. Li, C. Chen, W. Zhou, and Y. Li, "Transferability bound theory: Exploring relationship between adversarial transferability and flatness," *Advances in Neural Information Processing Systems*, vol. 37, pp. 41 882–41 908, 2024.
- [3] Y. Fang, Z. Wang, J. Cheng, R. Wang, and C. Liang, "Promoting adversarial transferability with enhanced loss flatness," in *2023 IEEE International Conference on Multimedia and Expo (ICME)*. IEEE, 2023, pp. 1217–1222.
- [4] X. Wang, J. Lin, H. Hu, J. Wang, and K. He, "Boosting adversarial transferability through enhanced momentum," *arXiv preprint arXiv:2103.10609*, 2021.
- [5] T. Wu, T. Luo, and D. C. Wunsch, "Gnp attack: Transferable adversarial examples via gradient norm penalty," in *2023 IEEE International Conference on Image Processing (ICIP)*. IEEE, 2023, pp. 3110–3114.
- [6] Y. Xu, Q. Chu, H. Yuan, Z. Luo, B. Liu, and N. Yu, "Enhancing adversarial transferability from the perspective of input loss landscape," in *International Conference on Image and Graphics*. Springer, 2023, pp. 254–266.
- [7] Z. Qin, Y. Fan, Y. Liu, L. Shen, Y. Zhang, J. Wang, and B. Wu, "Boosting the transferability of adversarial attacks with reverse adversarial perturbation," *Advances in neural information processing systems*, vol. 35, pp. 29 845–29 858, 2022.
- [8] Z. Ge, H. Liu, W. Xiaosen, F. Shang, and Y. Liu, "Boosting adversarial transferability by achieving flat local maxima," *Advances in Neural Information Processing Systems*, vol. 36, pp. 70 141–70 161, 2023.
- [9] K. He, X. Zhang, S. Ren, and J. Sun, "Deep residual learning for image recognition," in *Proceedings of the IEEE conference on computer vision and pattern recognition*, 2016, pp. 770–778.
- [10] C. Szegedy, W. Zaremba, I. Sutskever, J. Bruna, D. Erhan, I. Goodfellow, and R. Fergus, "Intriguing properties of neural networks," *arXiv preprint arXiv:1312.6199*, 2013.
- [11] I. J. Goodfellow, J. Shlens, and C. Szegedy, "Explaining and harnessing adversarial examples," *arXiv preprint arXiv:1412.6572*, 2014.
- [12] B. Biggio, I. Corona, D. Maiorca, B. Nelson, N. Šrđić, P. Laskov, G. Giacinto, and F. Roli, "Evasion attacks against machine learning at test time," in *Machine Learning and Knowledge Discovery in Databases: European Conference, ECML PKDD 2013, Prague, Czech Republic, September 23-27, 2013, Proceedings, Part III 13*. Springer, 2013, pp. 387–402.
- [13] N. Carlini and D. Wagner, "Towards evaluating the robustness of neural networks," in *2017 IEEE Symposium on Security and Privacy (SP)*. IEEE, 2017, pp. 39–57.
- [14] I. J. Goodfellow, J. Shlens, and C. Szegedy, "Explaining and harnessing adversarial examples," *arXiv preprint arXiv:1412.6572*, 2014.
- [15] A. Madry, A. Makelov, L. Schmidt, D. Tsipras, and A. Vladu, "Towards deep learning models resistant to adversarial attacks," *arXiv preprint arXiv:1706.06083*, 2017.
- [16] W. Brendel, J. Rauber, and M. Bethge, "Decision-based adversarial attacks: Reliable attacks against black-box machine learning models," *arXiv preprint arXiv:1712.04248*, 2017.
- [17] C. Guo, J. Gardner, Y. You, A. G. Wilson, and K. Weinberger, "Simple black-box adversarial attacks," in *International conference on machine learning*. PMLR, 2019, pp. 2484–2493.
- [18] J. Chen, M. I. Jordan, and M. J. Wainwright, "Hopskipjumpattack: A query-efficient decision-based attack," in *2020 IEEE Symposium on Security and Privacy (SP)*. IEEE, 2020, pp. 1277–1294.
- [19] C. Xie, Z. Zhang, Y. Zhou, S. Bai, J. Wang, Z. Ren, and A. L. Yuille, "Improving transferability of adversarial examples with input diversity," in *Proceedings of the IEEE/CVF conference on computer vision and pattern recognition*, 2019, pp. 2730–2739.
- [20] Y. Dong, T. Pang, H. Su, and J. Zhu, "Evading defenses to transferable adversarial examples by translation-invariant attacks," in *Proceedings of the IEEE/CVF conference on computer vision and pattern recognition*, 2019, pp. 4312–4321.
- [21] Y. Dong, F. Liao, T. Pang, H. Su, J. Zhu, X. Hu, and J. Li, "Boosting adversarial attacks with momentum," in *Proceedings of the IEEE conference on computer vision and pattern recognition*, 2018, pp. 9185–9193.
- [22] J. Lin, C. Song, K. He, L. Wang, and J. E. Hopcroft, "Nesterov accelerated gradient and scale invariance for adversarial attacks," *arXiv preprint arXiv:1908.06281*, 2019.

- [23] Y. Guo, Q. Li, and H. Chen, "Backpropagating linearly improves transferability of adversarial examples," *Advances in neural information processing systems*, vol. 33, pp. 85–95, 2020.
- [24] J. Zhang, W. Wu, J.-t. Huang, Y. Huang, W. Wang, Y. Su, and M. R. Lyu, "Improving adversarial transferability via neuron attribution-based attacks," in *Proceedings of the IEEE/CVF Conference on Computer Vision and Pattern Recognition*, 2022, pp. 14993–15002.
- [25] X. Wang, X. He, J. Wang, and K. He, "Admix: Enhancing the transferability of adversarial attacks," in *Proceedings of the IEEE/CVF International Conference on Computer Vision*, 2021, pp. 16158–16167.
- [26] Y. Long, Q. Zhang, B. Zeng, L. Gao, X. Liu, J. Zhang, and J. Song, "Frequency domain model augmentation for adversarial attack," in *European conference on computer vision*. Springer, 2022, pp. 549–566.
- [27] R. Zhu, Z. Zhang, S. Liang, Z. Liu, and C. Xu, "Learning to transform dynamically for better adversarial transferability," in *Proceedings of the IEEE/CVF Conference on Computer Vision and Pattern Recognition*, 2024, pp. 24273–24283.
- [28] Z. Yuan, J. Zhang, and S. Shan, "Adaptive image transformations for transfer-based adversarial attack," in *European Conference on Computer Vision*. Springer, 2022, pp. 1–17.
- [29] J. Zhang, J.-t. Huang, W. Wang, Y. Li, W. Wu, X. Wang, Y. Su, and M. R. Lyu, "Improving the transferability of adversarial samples by path-augmented method," in *Proceedings of the IEEE/CVF conference on computer vision and pattern recognition*, 2023, pp. 8173–8182.
- [30] D. Wu, Y. Wang, S.-T. Xia, J. Bailey, and X. Ma, "Skip connections matter: On the transferability of adversarial examples generated with resnets," *arXiv preprint arXiv:2002.05990*, 2020.
- [31] Y. Xiong, J. Lin, M. Zhang, J. E. Hopcroft, and K. He, "Stochastic variance reduced ensemble adversarial attack for boosting the adversarial transferability," in *Proceedings of the IEEE/CVF conference on computer vision and pattern recognition*, 2022, pp. 14983–14992.
- [32] H. Chen, Y. Zhang, Y. Dong, X. Yang, H. Su, and J. Zhu, "Rethinking model ensemble in transfer-based adversarial attacks," *arXiv preprint arXiv:2303.09105*, 2023.
- [33] M. Gubri, M. Cordy, M. Papadakis, Y. L. Traon, and K. Sen, "Lgv: Boosting adversarial example transferability from large geometric vicinity," in *European Conference on Computer Vision*. Springer, 2022, pp. 603–618.
- [34] Y. Zhang, S. Hu, L. Y. Zhang, J. Shi, M. Li, X. Liu, W. Wan, and H. Jin, "Why does little robustness help? a further step towards understanding adversarial transferability," in *2024 IEEE Symposium on Security and Privacy (SP)*. IEEE, 2024, pp. 3365–3384.
- [35] Q. Huang, I. Katsman, H. He, Z. Gu, S. Belongie, and S.-N. Lim, "Enhancing adversarial example transferability with an intermediate level attack," in *Proceedings of the IEEE/CVF international conference on computer vision*, 2019, pp. 4733–4742.
- [36] M. M. Naseer, S. H. Khan, M. H. Khan, F. Shahbaz Khan, and F. Porikli, "Cross-domain transferability of adversarial perturbations," *Advances in Neural Information Processing Systems*, vol. 32, 2019.
- [37] A. Kurakin, I. Goodfellow, and S. Bengio, "Adversarial machine learning at scale," *arXiv preprint arXiv:1611.01236*, 2016.
- [38] F. Tramèr, A. Kurakin, N. Papernot, I. Goodfellow, D. Boneh, and P. McDaniel, "Ensemble adversarial training: Attacks and defenses," *arXiv preprint arXiv:1705.07204*, 2017.
- [39] J. Cohen, E. Rosenfeld, and Z. Kolter, "Certified adversarial robustness via randomized smoothing," in *international conference on machine learning*. PMLR, 2019, pp. 1310–1320.
- [40] H. Salman, J. Li, I. Razenshteyn, P. Zhang, H. Zhang, S. Bubeck, and G. Yang, "Provably robust deep learning via adversarially trained smoothed classifiers," *Advances in neural information processing systems*, vol. 32, 2019.
- [41] F. Liao, M. Liang, Y. Dong, T. Pang, X. Hu, and J. Zhu, "Defense against adversarial attacks using high-level representation guided denoiser," in *Proceedings of the IEEE conference on computer vision and pattern recognition*, 2018, pp. 1778–1787.
- [42] C. Xie, Y. Wu, L. v. d. Maaten, A. L. Yuille, and K. He, "Feature denoising for improving adversarial robustness," in *Proceedings of the IEEE/CVF conference on computer vision and pattern recognition*, 2019, pp. 501–509.
- [43] M. Naseer, S. Khan, M. Hayat, F. S. Khan, and F. Porikli, "A self-supervised approach for adversarial robustness," in *Proceedings of the IEEE/CVF Conference on Computer Vision and Pattern Recognition*, 2020, pp. 262–271.
- [44] J. H. Metzen, T. Genewein, V. Fischer, and B. Bischoff, "On detecting adversarial perturbations," *arXiv preprint arXiv:1702.04267*, 2017.
- [45] W. Nie, B. Guo, Y. Huang, C. Xiao, A. Vahdat, and A. Anandkumar, "Diffusion models for adversarial purification," *arXiv preprint arXiv:2205.07460*, 2022.
- [46] N. Carlini and D. Wagner, "Adversarial examples are not easily detected: Bypassing ten detection methods," in *Proceedings of the 10th ACM workshop on artificial intelligence and security*, 2017, pp. 3–14.
- [47] J. Deng, W. Dong, R. Socher, L.-J. Li, K. Li, and L. Fei-Fei, "Imagenet: A large-scale hierarchical image database," in *2009 IEEE conference on computer vision and pattern recognition*. Ieee, 2009, pp. 248–255.
- [48] C. Szegedy, V. Vanhoucke, S. Ioffe, J. Shlens, and Z. Wojna, "Rethinking the inception architecture for computer vision," in *Proceedings of the IEEE conference on computer vision and pattern recognition*, 2016, pp. 2818–2826.
- [49] P. Foret, A. Kleiner, H. Mobahi, and B. Neyshabur, "Sharpness-aware minimization for efficiently improving generalization," *arXiv preprint arXiv:2010.01412*, 2020.
- [50] N. S. Keskar, D. Mudigere, J. Nocedal, M. Smelyanskiy, and P. T. P. Tang, "On large-batch training for deep learning: Generalization gap and sharp minima," *arXiv preprint arXiv:1609.04836*, 2016.
- [51] X. Zhang, R. Xu, H. Yu, H. Zou, and P. Cui, "Gradient norm aware minimization seeks first-order flatness and improves generalization," in *Proceedings of the IEEE/CVF Conference on Computer Vision and Pattern Recognition*, 2023, pp. 20247–20257.
- [52] D. Stutz, M. Hein, and B. Schiele, "Relating adversarially robust generalization to flat minima," in *Proceedings of the IEEE/CVF international conference on computer vision*, 2021, pp. 7807–7817.
- [53] A. Madry, A. Makelov, L. Schmidt, D. Tsipras, and A. Vladu, "Towards deep learning models resistant to adversarial attacks," *arXiv preprint arXiv:1706.06083*, 2017.
- [54] W. Zhou, X. Hou, Y. Chen, M. Tang, X. Huang, X. Gan, and Y. Yang, "Transferable adversarial perturbations," in *Proceedings of the European Conference on Computer Vision (ECCV)*, 2018, pp. 452–467.
- [55] M. Li, C. Deng, T. Li, J. Yan, X. Gao, and H. Huang, "Towards transferable targeted attack," in *Proceedings of the IEEE/CVF conference on computer vision and pattern recognition*, 2020, pp. 641–649.
- [56] Z. Zhao, Z. Liu, and M. Larson, "On success and simplicity: A second look at transferable targeted attacks," *Advances in Neural Information Processing Systems*, vol. 34, pp. 6115–6128, 2021.
- [57] C. Szegedy, S. Ioffe, V. Vanhoucke, and A. Alemi, "Inception-v4, inception-resnet and the impact of residual connections on learning," in *Proceedings of the AAAI conference on artificial intelligence*, vol. 31, 2017.
- [58] T. maintainers and contributors, "Torchvision: Pytorch's computer vision library," <https://github.com/pytorch/vision>, 2016, software.
- [59] G. Huang, Z. Liu, L. Van Der Maaten, and K. Q. Weinberger, "Densely connected convolutional networks," in *Proceedings of the IEEE conference on computer vision and pattern recognition*, 2017, pp. 4700–4708.
- [60] K. Simonyan and A. Zisserman, "Very deep convolutional networks for large-scale image recognition," *arXiv preprint arXiv:1409.1556*, 2014.
- [61] F. Chollet, "Xception: Deep learning with depthwise separable convolutions," in *Proceedings of the IEEE conference on computer vision and pattern recognition*, 2017, pp. 1251–1258.
- [62] M. Sandler, A. Howard, M. Zhu, A. Zhmoginov, and L.-C. Chen, "Mobilenetv2: Inverted residuals and linear bottlenecks," in *Proceedings of the IEEE conference on computer vision and pattern recognition*, 2018, pp. 4510–4520.
- [63] C. Liu, B. Zoph, M. Neumann, J. Shlens, W. Hua, L.-J. Li, L. Fei-Fei, A. Yuille, J. Huang, and K. Murphy, "Progressive neural architecture search," in *Proceedings of the European conference on computer vision (ECCV)*, 2018, pp. 19–34.
- [64] A. Dosovitskiy, L. Beyer, A. Kolesnikov, D. Weissenborn, X. Zhai, T. Unterthiner, M. Dehghani, M. Minderer, G. Heigold, S. Gelly *et al.*, "An image is worth 16x16 words: Transformers for image recognition at scale," *arXiv preprint arXiv:2010.11929*, 2020.
- [65] B. Heo, S. Yun, D. Han, S. Chun, J. Choe, and S. J. Oh, "Rethinking spatial dimensions of vision transformers," in *Proceedings of the IEEE/CVF international conference on computer vision*, 2021, pp. 11936–11945.
- [66] I. O. Tolstikhin, N. Houlsby, A. Kolesnikov, L. Beyer, X. Zhai, T. Unterthiner, J. Yung, A. Steiner, D. Keysers, J. Uszkoreit *et al.*, "Mlp-mixer: An all-mlp architecture for vision," *Advances in neural information processing systems*, vol. 34, pp. 24261–24272, 2021.
- [67] H. Touvron, P. Bojanowski, M. Caron, M. Cord, A. El-Nouby, E. Grave, G. Izacard, A. Joulin, G. Synnaeve, J. Verbeek *et al.*, "Resmlp: Feedforward networks for image classification with data-efficient training," *IEEE Transactions on Pattern Analysis and Machine Intelligence*, vol. 45, no. 4, pp. 5314–5321, 2022.

TABLE VI

TRANSFER ATTACK SUCCESS RATE (%) COMPARISON OF GRADIENT-STABILIZED ATTACKS ON CROSS-ARCHITECTURE MODELS. EVALUATING MEF_H/F AGAINST 12 GRADIENT STABILIZATION METHODS ON SEVEN DIVERSE ARCHITECTURES (CNNs, TRANSFORMERS, MLPs). THE BEST RESULTS ARE BOLD AND THE SECOND BEST RESULTS ARE UNDERLINED.

Attack	Res-50 \Rightarrow							Inc-v3 \Rightarrow						
	MobileNet	PNASNet-L	ViT-B/16	ViT-L/32	PiT-S	MLP-Mixer	ResMLP	MobileNet	PNASNet-L	ViT-B/16	ViT-L/32	PiT-S	MLP-Mixer	ResMLP
MI [21]	68.4	51.0	20.2	20.9	25.1	42.6	32.4	61.7	48.4	22.5	21.0	27.1	47.5	32.8
NI [22]	71.5	52.4	20.1	20.4	25.7	44.4	31.1	68.3	56.5	22.6	20.8	29.8	49.3	35.8
PI [4]	75.4	56.9	21.4	20.9	27.9	45.7	34.2	69.9	57.9	23.5	21.8	32.0	49.9	37.7
TPA [2]	74.9	58.5	23.6	23.8	30.7	47.6	36.6	63.7	57.1	23.6	21.2	28.9	50.7	37.0
GNP [5]	81.9	67.2	28.6	24.6	36.6	51.0	44.8	65.1	57.1	25.4	21.4	31.0	50.9	37.3
VMI [1]	84.3	70.2	33.8	28.1	45.4	51.3	51.9	71.8	65.0	35.8	27.7	45.0	54.1	49.1
VNI [1]	87.1	73.6	35.6	29.2	46.8	53.9	53.9	78.3	67.8	37.1	27.6	47.5	56.4	50.2
EMI [4]	88.2	70.8	27.6	24.7	37.4	50.7	45.3	81.5	69.5	32.2	24.7	41.5	56.6	48.0
RAP [7]	85.9	66.4	26.4	25.8	36.3	52.8	44.1	82.7	67.3	24.5	23.8	36.7	54.5	43.7
APP [6]	91.0	85.1	45.6	38.0	55.4	60.6	64.1	76.1	70.4	38.5	32.2	47.5	57.2	53.5
FEM [3]	94.0	87.0	43.1	35.0	58.1	60.2	66.0	81.1	78.2	41.3	30.4	53.2	59.7	58.6
PGN [8]	91.6	88.6	51.4	45.8	58.7	66.7	70.2	84.9	82.6	50.1	40.6	60.2	66.1	65.6
MEF_H	<u>95.2</u>	<u>90.3</u>	<u>51.9</u>	<u>46.0</u>	<u>63.3</u>	<u>66.9</u>	<u>70.5</u>	<u>85.2</u>	<u>83.9</u>	<u>51.7</u>	<u>42.2</u>	<u>60.4</u>	<u>67.3</u>	<u>66.3</u>
MEF_F	98.0	95.2	56.0	46.9	71.1	71.7	77.4	92.7	90.8	56.2	45.3	71.4	69.4	73.3

TABLE VII

TRANSFER ATTACK SUCCESS RATE (%) COMPARISON ON ENSEMBLE SURROGATES. USING LOGITS-AVERAGED RES-50 AND INC-V3 AS SURROGATE MODELS, OUR MEF_H/F VARIANTS OUTPERFORM 12 GRADIENT-STABILIZED ATTACKS AND TWO ENSEMBLE-SPECIALIZED METHODS (SVRE [31], CWA [32]). THE BEST RESULTS ARE BOLD AND THE SECOND BEST RESULTS ARE UNDERLINED.

Attack	Res-50 + Inc-v3 \Rightarrow													
	Res-101	Inc-v4	IncRes-v2	Inc-v3 _{adv}	Inc-v3 _{ens3}	Inc-v3 _{ens4}	IncRes-v2 _{ens}	MobileNet	PNASNet-L	ViT-B/16	ViT-L/32	PiT-S	MLP-Mixer	ResMLP
MI [21]	94.1	68.3	56.1	33.6	30.4	30.7	16.9	76.6	63.4	32.7	25.4	39.1	51.6	47.9
NI [22]	96.8	71.4	61.8	36.4	33.2	30.4	16.2	80.6	66.6	32.7	24.7	42.6	54.2	49.7
PI [4]	98.0	78.2	68.8	38.4	34.7	34.5	19.2	83.5	72.9	35.1	25.8	47.7	54.6	54.4
TPA [2]	90.3	63.6	54.1	27.8	20.8	20.1	12.4	72.1	60.3	29.6	25.1	39.1	50.5	43.7
GNP [5]	92.8	73.4	66.9	37.1	32.1	30.8	17.1	76.9	66.5	32.5	25.7	45.9	52.8	51.0
VMI [1]	97.6	83.4	77.3	54.8	55.3	54.6	37.1	87.4	80.7	49.0	35.1	62.1	62.0	66.2
VNI [1]	98.9	86.5	80.3	58.5	57.2	56.4	37.8	90.1	82.5	50.2	35.7	65.2	62.3	68.4
EMI [4]	<u>99.1</u>	90.9	83.2	51.9	46.6	44.6	25.7	93.1	85.9	45.1	32.8	62.8	61.8	69.3
RAP [7]	98.4	86.1	80.5	42.3	28.0	24.9	14.0	92.4	80.8	42.3	31.1	58.1	63.7	65.8
APP [6]	97.8	88.3	84.6	64.2	63.1	63.3	47.1	88.9	84.5	54.2	42.6	67.1	65.2	73.8
FEM [3]	98.7	92.0	88.3	68.3	65.9	62.9	46.9	92.5	89.0	59.0	41.3	74.1	66.0	77.0
SVRE [31]	92.0	69.2	58.8	31.0	26.5	26.6	13.2	77.8	64.0	29.0	23.5	41.1	50.7	47.4
CWA [32]	94.9	53.8	45.3	26.3	16.3	14.5	8.0	74.6	56.5	20.8	20.9	26.3	49.0	34.2
PGN [8]	97.8	91.9	89.4	79.5	78.2	77.5	65.6	93.9	91.9	68.7	50.2	76.9	74.5	81.8
MEF_H	98.9	<u>93.2</u>	<u>90.2</u>	<u>80.2</u>	<u>79.8</u>	<u>80.5</u>	<u>67.0</u>	<u>94.1</u>	<u>92.4</u>	<u>69.5</u>	<u>51.7</u>	<u>77.8</u>	<u>75.3</u>	<u>82.1</u>
MEF_F	99.4	96.6	95.1	85.7	83.3	82.6	70.4	96.7	95.1	75.4	55.2	83.8	80.4	89.0

SUPPLEMENTARY MATERIAL

A. Evaluation on Diverse Network Architectures

To assess cross-architecture transferability, we generate adversarial examples on Res-50 [9] and Inc-v3 [48] surrogate models, then evaluate success rates across seven diverse architectures: (1) CNNs (MobileNet-v2 [62], PNASNet-5-Large [63]), (2) Transformers (ViT-B/16 [64], ViT-L/32 [64], PiT-S [65]), and (3) MLPs (MLP-Mixer [66], ResMLP [67]).

Table VI compares $\text{MEF}_H/\text{MEF}_F$ against 12 gradient stabilization baselines. Despite using half the computational budget, MEF_H achieves 67.29% average success rate across all architectures, surpassing PGN [8]’s 65.94% full-cost performance. When matching PGN’s computational expense, MEF_F elevates the average success rate to 72.39%, a 6.45% absolute improvement. The results validate that adversarial examples crafted via our framework maintain high transferability even when targeting models with fundamentally different inductive biases, establishing new state-of-the-art generalization across architectural paradigms.

B. Attacking on Ensemble of Models

We extend evaluation to ensemble attacks by integrating Inc-v3 [48] and Res-50 [9] through logit averaging, generating adversarial examples against this combined surrogate. To comprehensively assess ensemble attack performance, we compare our method against 12 representative gradient stabilization attacks and two ensemble-specialized approaches (SVRE [31], CWA [32]). The transferability

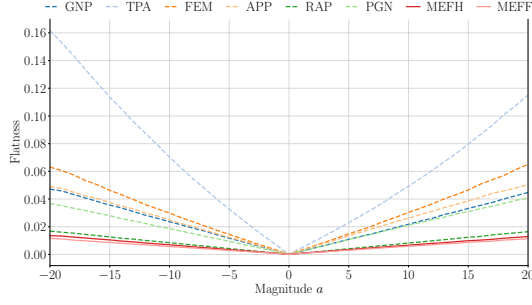
of these examples is then tested across defended models and cross-architecture targets.

As shown in Table VII, MEF_H surpasses PGN’s performance across all target models while requiring only half the computational budget. When matching PGN’s budget, MEF_F demonstrates consistent superiority, outperforming PGN by 1.6-8.2% across individual models. The results confirm that our framework inherently captures transferable adversarial patterns across surrogate ensembles without requiring specialized ensemble strategies, achieving state-of-the-art transferability.

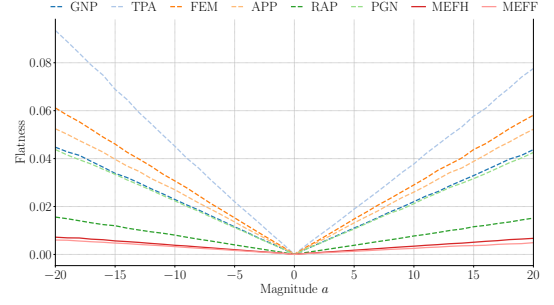
C. Flatness Comparison

To validate that MEF_H and MEF_F achieve enhanced flatness for transferable adversarial examples, we adopt the evaluation framework from RAP [7]. First, random directions are sampled from a Gaussian distribution and normalized to an ℓ_2 -norm sphere to ensure uniform exploration. We then compute loss variations between original and perturbed samples across perturbation magnitudes ranging from -20 to 20 . For robust estimation, each magnitude level employs 20 randomly sampled directions to reduce measurement variance. The results on Res-50 [9] and Inc-v3 [48] are shown in Figure 5, MEF_H and MEF_F achieves the lowest loss variations.

For quantitative analysis, we estimate the zeroth-order and first-order flatness ($\bar{R}_\xi^{(0)}(\mathbf{x})$ and $\bar{R}_\xi^{(1)}(\mathbf{x})$) via Monte Carlo sampling with exploration radius $\xi = 32/255$. Using 128 samples per example ensures metric stability, outperforming the 20-sample baseline in precision. Table VIII shows that MEF_H achieves the lowest $\bar{R}_\xi^{(0)}(\mathbf{x})$ across all models, while MEF_F further minimizes $\bar{R}_\xi^{(1)}(\mathbf{x})$ through extended optimization. Despite focusing on zeroth-order flatness, MEF_F



(a) ResNet-50 [9]



(b) Inc-v3 [48]

Fig. 5. The flatness visualization of adversarial examples via ℓ_2 -constrained perturbation analysis. Evaluating MEF_H and MEF_F on Res-50 [9] and Inc-v3 [48] with random directional perturbations (magnitude range: $[-20, 20]$).

TABLE VIII
QUANTITATIVE COMPARISON OF ZERO/TH/FIRST-ORDER FLATNESS METRICS ($\overline{R}_\xi^{(n)}$). THE BEST FLATNESS ARE BOLD.

Attack \ Model	VMI [1]	VNI [1]	EMI [4]	RAP [7]	GNP [5]	FEM [3]	APP [6]	TPA [2]	PGN [8]	MEF_H	MEF_F
Res-50 [9]	29.03 / 0.49	23.04 / 0.41	25.57 / 0.45	15.98 / 0.45	50.49 / 0.53	12.20 / 0.55	2.41 / 0.47	2.71 / 0.18	2.93 / 0.37	2.20 / 0.26	2.34 / 0.10
Res-101 [9]	25.44 / 0.50	20.24 / 0.41	21.32 / 0.46	13.13 / 0.45	46.37 / 0.57	10.01 / 0.55	2.64 / 0.44	2.45 / 0.17	3.09 / 0.36	2.06 / 0.19	2.21 / 0.11
Inc-v3 [48]	8.32 / 0.64	7.74 / 0.59	8.77 / 0.62	7.80 / 0.62	29.37 / 0.86	3.52 / 0.79	1.75 / 0.65	1.24 / 0.27	2.11 / 0.56	1.09 / 0.27	1.06 / 0.21
Inc-v4 [57]	4.71 / 0.50	4.12 / 0.43	5.01 / 0.46	3.71 / 0.46	16.06 / 0.68	2.71 / 0.56	1.48 / 0.53	2.40 / 0.41	1.40 / 0.48	0.79 / 0.32	0.84 / 0.29

inherently optimizes both metrics, reducing $\overline{R}_\xi^{(1)}(\mathbf{x})$ over baselines as iterations increase. These results confirm the strong correlation between flatness minimization and transferability enhancement, validating our theoretical foundation.